

Renormalization of domain-wall bilinear operators with short-distance current correlators

M. Tomii,^{1,2,*} G. Cossu,² B. Fahy,² H. Fukaya,³
S. Hashimoto,^{1,2} T. Kaneko,^{1,2} and J. Noaki²

(JLQCD collaboration)

¹*Department of Particle and Nuclear Science,
SOKENDAI (The Graduate University for Advanced Studies), Tsukuba 305-0801, Japan*

²*Theory Center, Institute of Particle and Nuclear Studies,
High Energy Accelerator Research Organization (KEK), Tsukuba 305-0801, Japan*

³*Department of Physics, Osaka University, Toyonaka 560-0043, Japan*

Abstract

We determine the renormalization constants for flavor non-singlet fermion bilinear operators of Möbius domain-wall fermions. The renormalization condition is imposed on the correlation functions in the coordinate space, such that the non-perturbative lattice calculation reproduces the perturbatively calculated counterpart at short distances. The perturbative expansion is precise as the coefficients are available up to $O(\alpha_s^4)$. We employ 2 + 1-flavor lattice ensembles at three lattice spacings in the range 0.044–0.080 fm.

* tomii@post.kek.jp

I. INTRODUCTION

Renormalization of lattice operators is a necessary step for the lattice QCD calculations of scheme-dependent quantities such as the matrix elements of the weak effective Hamiltonian, which contains composite operators of quark fields such as bilinear and four-fermion operators. In phenomenological studies, comparison of lattice results with experimental values or theoretical results from other approaches has to be performed with a matched renormalization scheme and scale. The conventional choice for this is the $\overline{\text{MS}}$ scheme. Among bilinear operators, vector (and axial-vector) currents are simplest because they are not renormalized because of current conservation. On the lattice, however, the commonly used local vector current is not conserved at finite lattice spacing and a finite renormalization to match the continuum counterpart is necessary. The axial-current is renormalized differently unless the lattice fermion formulation respects chiral symmetry. Scale dependent operators such as scalar and pseudoscalar currents require renormalization in any case.

Matching to the continuum renormalization scheme necessarily involves perturbation theory, since the $\overline{\text{MS}}$ scheme adopted in the continuum theory is inherently perturbative. It means that the renormalization condition must be applied at momentum scale of 2 GeV or higher, where QCD becomes perturbative. In this regime, the discretization effect of lattice theory becomes significant as typical value of lattice cutoff for currently available ensembles is 2–3 GeV. This causes the so-called window problem, which implies that one has to identify a window of momentum scale where the systematic uncertainties of perturbative and lattice calculations are controlled. One of the widely used method is the non-perturbative renormalization through the RI/MOM scheme as an intermediate renormalization condition [1]. In this method, one calculates the vertex function involving the composite operator of interest with a certain momentum configuration of external quarks in a fixed gauge. The external momenta are carefully chosen to satisfy the window condition as mentioned above. In many cases, one can find the region where the discretization effect is under control by inspecting the momentum dependence of the obtained vertex function. The convergence of the perturbative expansion, on the other hand, is not well tested, as the perturbative expansion is available only at the one- or two-loop level in many cases. In fact, this is a dominant source of systematic uncertainty in this method.

In this work, we adopt another renormalization condition, which is called the coordinate

space method or the X-space method. The method was first proposed in [2] and has so far been applied in [3, 4]. In this method, the renormalization condition is imposed on the correlation function at a certain distance in the coordinate space. The correlation functions are those of composite operators of interest. A typical example is a correlation function of vector currents $\bar{u}\gamma_\mu d(x)$ and $\bar{d}\gamma_\nu u(y)$ placed at certain points x and y in the coordinate space. Here, u and d denote the up and down quark fields, respectively. The correlation function thus constructed $\langle \bar{u}\gamma_\mu d(x)\bar{d}\gamma_\nu u(y) \rangle$ is gauge invariant, and more importantly it is a common object in the continuum QCD for which the state-of-the-art techniques of perturbative QCD have been applied. For the (axial-)vector and (pseudo)scalar correlators, the perturbative series has been calculated to the order of α_s^4 [5], with which the uncertainty due to a truncation of the perturbative series is highly suppressed and the remaining uncertainty is reliably estimated using the convergence behavior of the series. Another important advantage of the X-space method is that the X-space correlator does not involve extra divergences other than those of the operators involved, because of the finite distance between x and y . The corresponding correlator in the momentum space has an extra divergence from a loop contracting the two points, and one has to consider a derivative in the momentum space to extract a well-defined quantity.

The window problem does exist for the X-space method. The distance between x and y must be sufficiently small for perturbation theory to be convergent, and at the same time it has to be large compared to the lattice spacing a . The main point of this work is therefore to identify such a region. On the perturbative side, we investigate the convergence property of the perturbative series known to α_s^4 . The convergence can be improved by optimizing the scale μ of coupling constant $\alpha_s(\mu)$, depending on the distance $|x - y|$. We first attempt the use of the Brodsky-Lepage-Mackenzie (BLM) scale setting procedure [6], which in fact leads to a much improved convergence compared to a naïve choice of $\mu = 1/|x - y|$. In order to estimate the remaining uncertainty due to the truncation of higher order terms, we vary the scale in some range and inspect the stability of the result. A detailed account of this study is given in Section III for both vector and scalar correlators.

As we include the longer-distance correlators in the analysis, non-perturbative power corrections could also appear as well as the problem of increasingly less convergent perturbative series. Such effect is described by the Operator Product Expansion (OPE) [7]. The leading contribution comes from the dimension-four operators: the quark condensate

and gluon condensate. The quark condensate appears with a quark mass, and induces a linear dependence on the quark mass. We confirm that the lattice data are consistent with the prediction of OPE. We can then eliminate this type of power correction by combining vector and axial-vector correlators with appropriate factors. Similar method is also applied for scalar and pseudoscalar correlators. The effect of gluon condensate is more difficult to identify. We fit the lattice data to the corresponding functional form in $|x - y|$.

At short distances on the lattice, the discretization error is a major concern, which we investigate in detail in Section IV. The discretization effect is indeed very substantial at the distance of $|x - y|/a \lesssim 10$. Fortunately, most of such effects can be eliminated by subtracting the correlators calculated at the tree-level (or mean-field improved). Further reduction can be achieved by selecting the direction of the points on the lattice. These improvements have already been applied in the previous studies [3, 4], and we refine them to minimize the remaining errors. Even after such reductions of errors, the discretization effects are still significant at the level of 3–5% for the correlators. We attempt to eliminate them by using the lattice data available for us at three different lattice spacings in the range 0.044–0.080 fm. We fit the lattice data at short distances assuming that the leading discretization effect is $O(a^2)$, and subtract it. The remaining error is then at the level of one per cent.

In this work, we determine the renormalization constants for the vector (and axial-vector) current and scalar (and pseudoscalar) density operator composed of the Möbius domain-wall fermions [8, 9]. Möbius domain-wall fermion is an improved implementation of the domain-wall fermion [10, 11]. The four-dimensional effective Dirac operator of the domain-wall fermion precisely satisfies the Ginsparg-Wilson relation and thus respects the modified chiral symmetry on the lattice. It implies that the vector and axial-vector renormalization factors are equal to each other to a good precision. With the Möbius implementation, the residual mass, which quantifies the size of the Ginsparg-Wilson violation, is at the order of 1 MeV or less on our lattice ensembles. For the determination of the renormalization constants, this amount of violation can be safely neglected. In fact, we confirm that the corresponding current correlators agree very precisely at short distances where the effect of the quark condensate is negligible.

This paper is organized as follows. In Section II, we describe the basic strategy to determine the renormalization constants. In Section III, we discuss the detail of massless correlators in perturbation theory and the improvement of their convergence. After that,

we give the contribution of OPE to the correlators. In Section IV, we show the analyses of lattice calculation including our lattice setup and some managements of lattice artifacts. In Section V, we explain the detail of determination of the renormalization factors and show the final results.

II. RENORMALIZATION CONDITION IN THE X-SPACE METHOD

In the X-space method, the renormalization constants are determined by analyzing two-point correlation functions at finite separation $x - y$. In this work, we consider the following four channels of flavor non-singlet correlators in the coordinate space,

$$\begin{aligned}\Pi_S(x) &= \langle S(x)S(0)^\dagger \rangle, & \Pi_P(x) &= \langle P(x)P(0)^\dagger \rangle, \\ \Pi_V(x) &= \sum_\mu \langle V_\mu(x)V_\mu(0)^\dagger \rangle, & \Pi_A(x) &= \sum_\mu \langle A_\mu(x)A_\mu(0)^\dagger \rangle,\end{aligned}\tag{1}$$

where each operator is composed of (mass degenerate) up and down quark fields $u(x)$ and $d(x)$,

$$\begin{aligned}S(x) &= \bar{u}(x)d(x), & P(x) &= \bar{u}(x)i\gamma_5d(x), \\ V_\mu(x) &= \bar{u}(x)\gamma_\mu d(x), & A_\mu(x) &= \bar{u}(x)\gamma_\mu\gamma_5d(x).\end{aligned}\tag{2}$$

Here, the coordinate y of the source point is fixed at origin and correlators are parametrized by a four-dimensional coordinate x with an assumption of translational invariance.

We renormalize the quark bilinear operators on the lattice to those in the $\overline{\text{MS}}$ scheme at a renormalization scale, which is often set to 2 or 3 GeV. Neglecting the contributions of irrelevant operators, the renormalization is multiplicative, *i.e.*

$$O_\Gamma^{\overline{\text{MS}}}(2 \text{ GeV}; x) = Z_\Gamma^{\overline{\text{MS}}/\text{lat}}(2 \text{ GeV}, a)O_\Gamma^{\text{lat}}(a; x),\tag{3}$$

where $\Gamma \in \{S, P, V, A\}$, $O_\Gamma \in \{S, P, V_\mu, A_\mu\}$, and $Z_\Gamma^{\overline{\text{MS}}/\text{lat}}(2 \text{ GeV}, a)$ is the renormalization constant. The renormalization condition in the X-space method is imposed by requiring

$$\left(\tilde{Z}_\Gamma^{\overline{\text{MS}}/\text{lat}}(2 \text{ GeV}, a; x)\right)^2 \Pi_\Gamma^{\text{lat}}(a; x) = \Pi_\Gamma^{\overline{\text{MS}}}(2 \text{ GeV}; x),\tag{4}$$

or

$$\tilde{Z}_\Gamma^{\overline{\text{MS}}/\text{lat}}(2 \text{ GeV}, a; x) = \sqrt{\frac{\Pi_\Gamma^{\overline{\text{MS}}}(2 \text{ GeV}; x)}{\Pi_\Gamma^{\text{lat}}(a; x)}},\tag{5}$$

at a finite distance x . Note that $\tilde{Z}_\Gamma^{\overline{\text{MS}}/\text{lat}}(2 \text{ GeV}, a; x)$ still contains some dependence on x . It originates from errors arising in the continuum $\Pi_\Gamma^{\overline{\text{MS}}}(2 \text{ GeV}; x)$ and lattice $\Pi_\Gamma^{\text{lat}}(a; x)$

correlators. The continuum one suffers from truncation of the perturbative expansion as we discuss in the following sections. On the other hand, the lattice correlator contains discretization effects. In addition, the x -dependence of $\widetilde{Z}_\Gamma^{\overline{\text{MS}}/\text{lat}}(2 \text{ GeV}, a; x)$ is also caused by non-perturbative effects at large $|x|$ in full QCD, which are not encoded in the continuum perturbative correlator. In order to extract the renormalization constant, which must be independent of x , the distance $|x|$ of correlators should be chosen in a window $a \ll |x| \ll 1/\Lambda_{\text{QCD}}$ to suppress these possible errors. In Section V, the systematic effects arising in $\widetilde{Z}_\Gamma^{\overline{\text{MS}}}(2 \text{ GeV}, a; x)$ are discussed in more detail and the renormalization factor $Z_\Gamma^{\overline{\text{MS}}}(2 \text{ GeV}, a)$ is determined.

III. CONTINUUM THEORY

A. Massless perturbation theory

In this subsection, we discuss the convergence of the perturbative expansion of the massless correlators. Since the scalar and pseudoscalar correlators, as well as the vector and axial-vector correlators, degenerate in the massless perturbation theory, *i.e.* $\Pi_S = \Pi_P$ and $\Pi_V = \Pi_A$, we consider only the two channels Π_S and Π_V .

The perturbative expansion of the vector correlator is written as

$$\Pi_V^{\overline{\text{MS}}}(x) = \frac{6}{\pi^4 x^6} \left(1 + \sum_{i=1}^{\infty} C_i^V a_s(\mu_x)^i \right), \quad (6)$$

with perturbative coefficients C_i^V . Here, $a_s(\mu_x) = \alpha_s(\mu_x)/\pi$ is the strong coupling constant and its scale μ_x is set as

$$\mu_x = \frac{1}{|x|}. \quad (7)$$

One can reorganize the perturbative series using the renormalization group to another scale μ_x^* , *i.e.*

$$\Pi_V^{\overline{\text{MS}}}(x) = \frac{6}{\pi^4 x^6} \left(1 + \sum_{i=1}^{\infty} C_i^V(\mu_x^*) a_s(\mu_x^*)^i \right), \quad (8)$$

which is exact when the perturbative series includes all orders, provided that the coefficients $C_i^V(\mu_x^*)$ are converted appropriately. The conversion formula of the coupling constants is available to four-loop level [12].

Chetyrkin and Maier [5] wrote the perturbative coefficients up to $O(a_s^4)$ at the renormalization scale μ_x in the $\widetilde{\text{MS}}$ scheme, which is the same as the $\overline{\text{MS}}$ scheme at a scale

$\tilde{\mu}_x = 2e^{-\gamma_E} \mu_x \simeq 1.123/|x|$. Here, $\gamma_E = 0.5772\dots$ is Euler's constant. In our notation, these coefficients correspond to $C_i^V(\tilde{\mu}_x)$. The perturbative coefficients $C_i^V(\mu_x^*)$ at $\mu_x^* = \mu_x, \tilde{\mu}_x$ obtained by using the results of [5] and [12] are summarized in Appendix A.

Since the perturbative expansion truncated at a finite order may depend on μ_x^* , there is an optimal choice for the scale that leads to a good convergence. One possible recipe to choose the optimal scale μ_x^* is the Brodsky-Lepage-Mackenzie (BLM) approach [6], which is motivated by an idea of absorbing the higher order contributions of gluon vacuum polarization into the coupling constant. The scale is chosen such that the perturbative coefficient at a_s^2 becomes independent of the number of flavors n_f . This BLM scale μ_x^{BLM} of the vector correlator thus determined is

$$\mu_x^{\text{BLM}} = 2 \exp \left[\frac{1}{2}(4\zeta_3 - 3 - 2\gamma_E) \right] \mu_x \simeq \frac{2.7733}{|x|}, \quad (9)$$

where $\zeta_3 \simeq 1.2021$. The perturbative coefficients $C_i^V(\mu_x^{\text{BLM}})$ at the BLM scale are summarized in Appendix A.

Figure 1 shows the vector correlator calculated with $\mu_x^* = \mu_x$ and $n_f = 3$. It is normalized by the tree-level correlator $\Pi_V^{\text{free}}(x) = 6/\pi^4 x^6$. A reasonable convergence is observed only below $|x| \sim 0.15$ fm, which is not so large compared to our lattice spacings $a = 0.044$ – 0.080 fm. It implies that there is no renormalization window satisfying the condition that the perturbative calculation is convergent and the discretization effects are sufficiently small. The convergence of the perturbative series at $\mu_x^* = \tilde{\mu}_x$ is similar to that at $\mu_x^* = \mu_x$. On the other hand, the result at $\mu_x^* = \mu_x^{\text{BLM}}$ with $n_f = 3$ shows much better convergence as plotted in Fig. 2, implying that the convergence of the perturbative series is actually improved by tuning the renormalization scale μ_x^* .

In order to choose the optimal scale and estimate the uncertainty of the higher order corrections, we investigate the μ_x^* -dependence of the perturbative calculation. The μ_x^* -dependence of the vector correlator with $n_f = 3$ is shown in Fig. 3 for several distances in the range 0.2–0.5 fm. Since the all-order calculation has to be independent of μ_x^* , we determine the optimal scale $\mu_x^{*,\text{opt}}$ as the value which minimizes the μ_x^* -derivative of the four-loop correlator,

$$\mu_x^{*,\text{opt}} = e^{1.7} \mu_x \simeq \frac{5.5}{|x|}. \quad (10)$$

The uncertainty of the higher order corrections to the vector correlator is estimated by varying μ_x^* in the region $[\frac{1}{2}\mu_x^{*,\text{opt}}, 2\mu_x^{*,\text{opt}}]$, which is shown in Fig. 3 by the gray band.

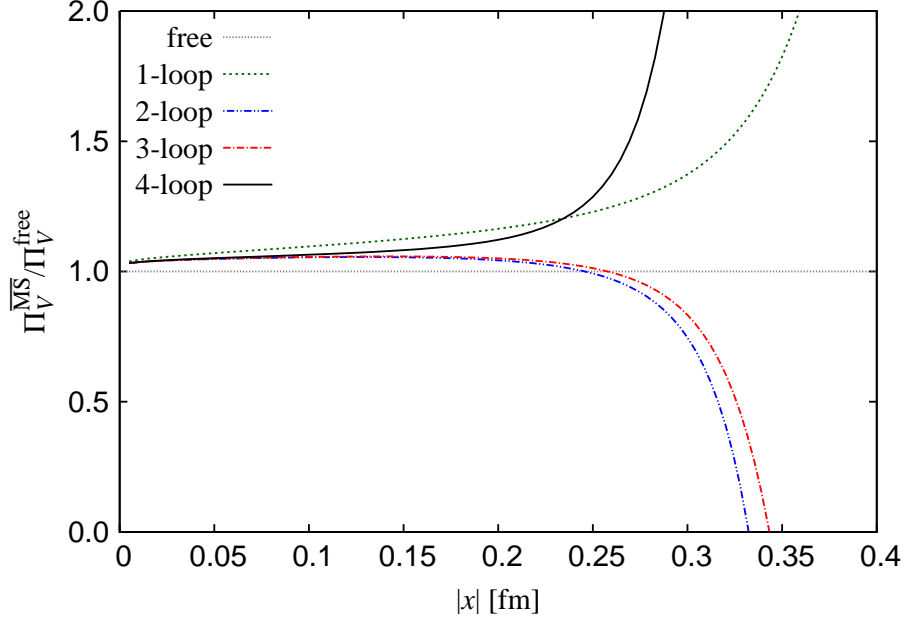


FIG. 1. Perturbative expansion of the vector correlator renormalized in the $\overline{\text{MS}}$ scheme with $n_f = 3$. The results at $\mu_x^* = \mu_x$ truncated at a_s^0 (fine-dotted), a_s (dotted), a_s^2 (dashed double-dotted), a_s^3 (dashed dotted), and a_s^4 (solid) are plotted as functions of $|x|$.

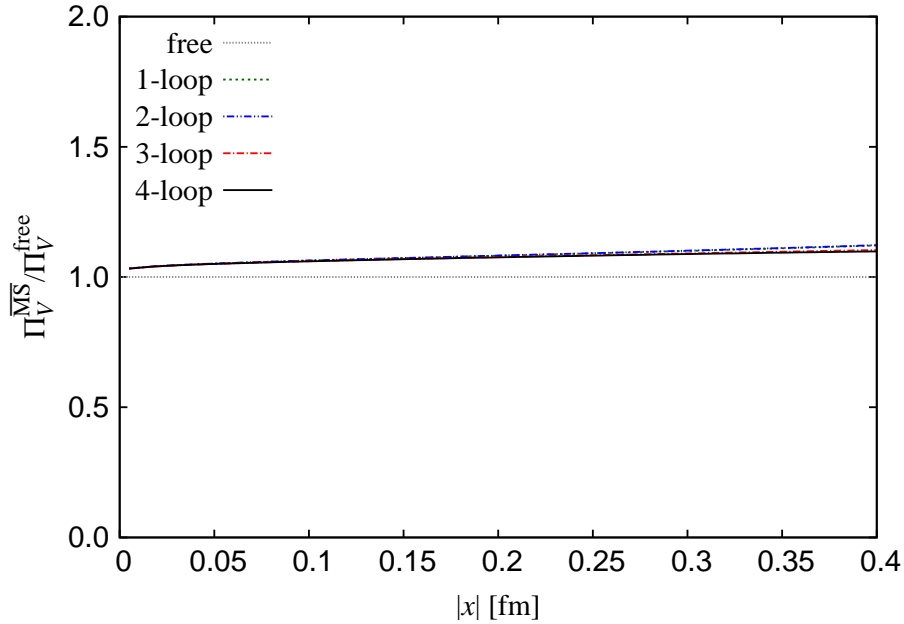


FIG. 2. Perturbative expansion of the vector correlator renormalized in the $\overline{\text{MS}}$ scheme with $n_f = 3$. The results at $\mu_x^* = \mu_x^{\text{BLM}}$ truncated at a_s^0 (fine-dotted), a_s (dotted), a_s^2 (dashed double-dotted), a_s^3 (dashed dotted), and a_s^4 (solid) are plotted as functions of $|x|$.

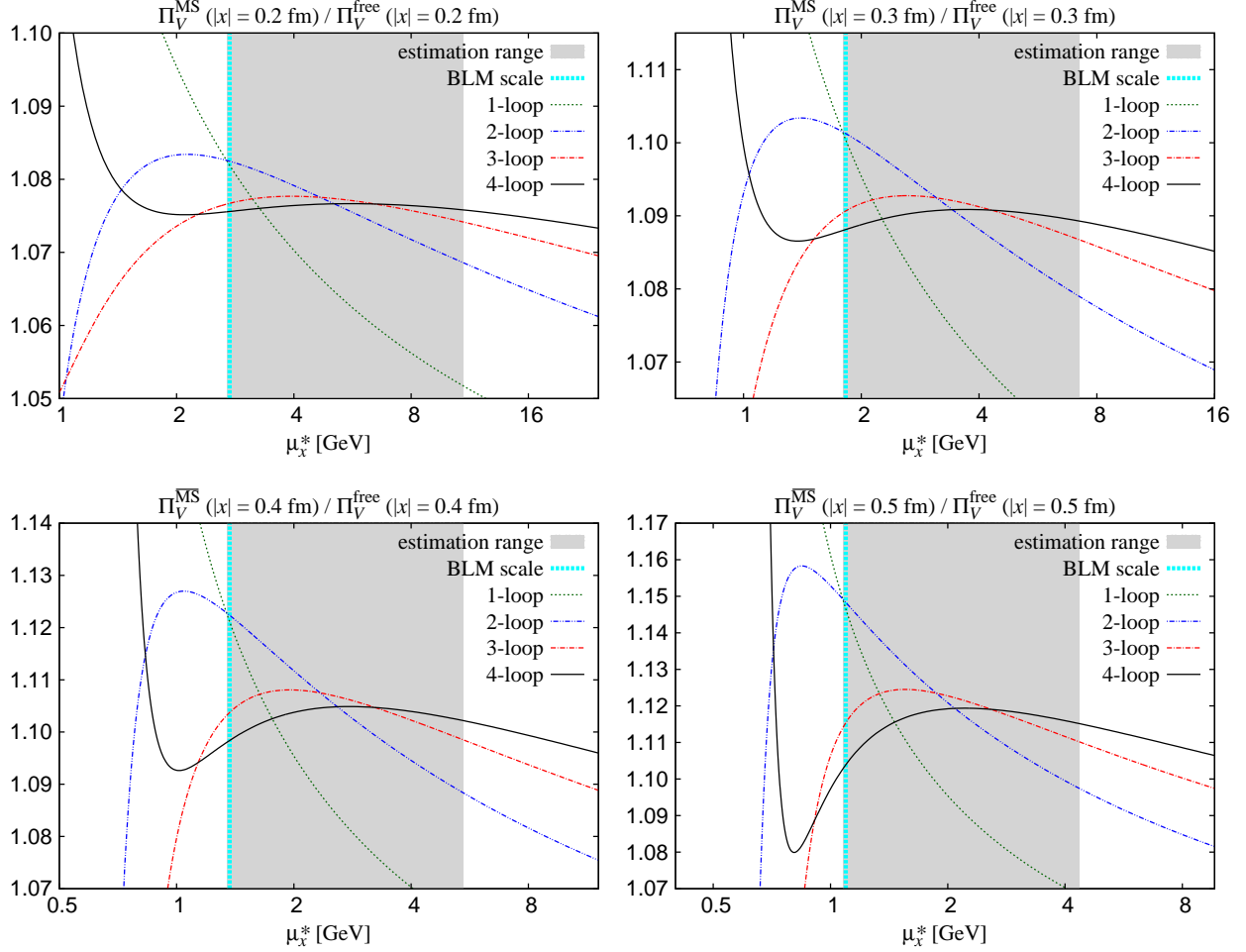


FIG. 3. Vector correlator renormalized in the $\overline{\text{MS}}$ scheme at the specific distances 0.2 fm (top/left), 0.3 fm (top/right), 0.4 fm (bottom/left), and 0.5 fm (bottom/right) as functions of μ_x^* . The results with $n_f = 3$ truncated at a_s (dotted), a_s^2 (dashed double-dotted), a_s^3 (dashed dotted), and a_s^4 (solid) are plotted. The gray band represents the region in which we estimate the uncertainty of the higher order corrections. The vertical bold line near the lower end of the gray band stands for the BLM scale (9).

The expansion at the scale $\mu_x^{*,\text{opt}}$ reads

$$\Pi_V^{\overline{\text{MS}}}(x) \Big|_{n_f=3} = \frac{6}{\pi^4 x^6} \left(1 + a_s(\mu_x^{*,\text{opt}}) + 3.1431 a_s(\mu_x^{*,\text{opt}})^2 + 4.8432 a_s(\mu_x^{*,\text{opt}})^3 - 33.819 a_s(\mu_x^{*,\text{opt}})^4 + O(a_s^5) \right). \quad (11)$$

As shown in Fig. 4, the choice of $\mu_x^{*,\text{opt}}$ shows better convergence. The gray region in the figure represents the higher order uncertainty, which is estimated by the maximum difference

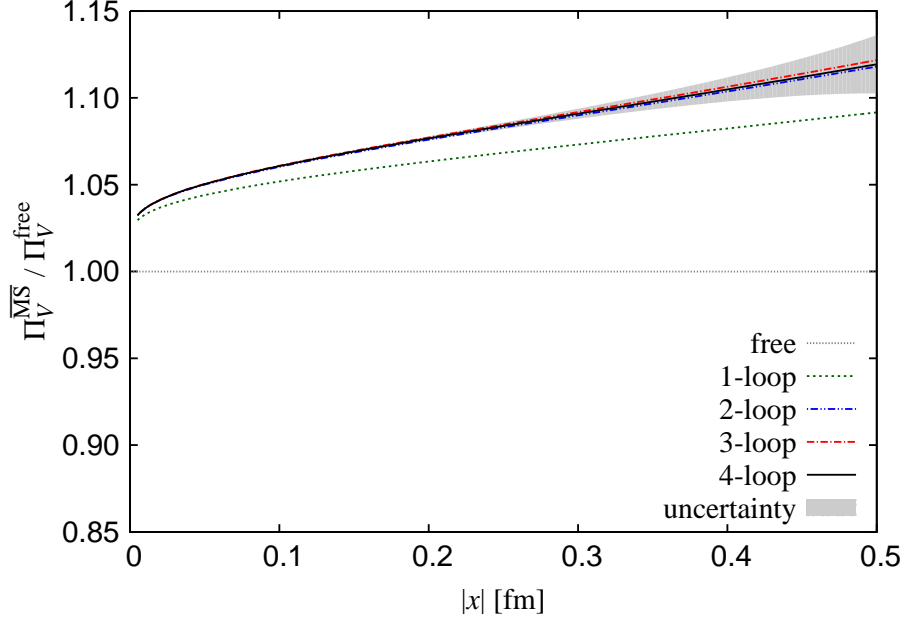


FIG. 4. Perturbative expansion of the vector correlator renormalized in the $\overline{\text{MS}}$ scheme with $n_f = 3$. The results of the perturbative series (11) at the optimal scale $\mu_x^* = \mu_x^{*,\text{opt}}$ truncated at a_s^0 (fine-dotted), a_s (dotted), a_s^2 (dashed double-dotted), a_s^3 (dashed dotted), and a_s^4 (solid) are plotted as functions of $|x|$.

between the correlator at $\mu_x^* = \mu_x^{*,\text{opt}}$ and those at μ_x^* in $[\frac{1}{2}\mu_x^{*,\text{opt}}, 2\mu_x^{*,\text{opt}}]$.

Next, we consider the scalar correlator. The scalar channel is more complicated due to the scale dependence of the scalar operator $S(x)$. Using the beta function [12] and the anomalous dimension [13, 14], we can treat a general expression of the perturbative expansion of the scalar correlator, which is written as

$$\Pi_S^{\overline{\text{MS}}}(\mu_x'; x) = \frac{3}{\pi^4 x^6} \left(1 + \sum_{i=1}^{\infty} C_i^S(\mu_x^*, \mu_x') a_s(\mu_x^*)^i \right), \quad (12)$$

where the first argument μ_x^* of the perturbative coefficients is the renormalization scale of the strong coupling constant in the perturbative series and the second μ_x' is the renormalization scale of the scalar operator. Chetyrkin and Maier [5] gave the perturbative coefficients of correlators at the renormalization scale $\mu_x^* = \mu_x' = \tilde{\mu}_x$, which is $C_i^S(\tilde{\mu}_x, \tilde{\mu}_x)$ in our notation. The coefficients $C_i^S(\mu_x, \mu_x)$ and $C_i^S(\tilde{\mu}_x, \tilde{\mu}_x)$ are summarized in Appendix A.

Figure 5 shows the convergence of the perturbative expansion at $\mu_x^* = \mu_x' = \mu_x$ with $n_f = 3$. The correlator in the figure is normalized by the tree-level one, $\Pi_S^{\text{free}}(x) = 3/\pi^4 x^6$.

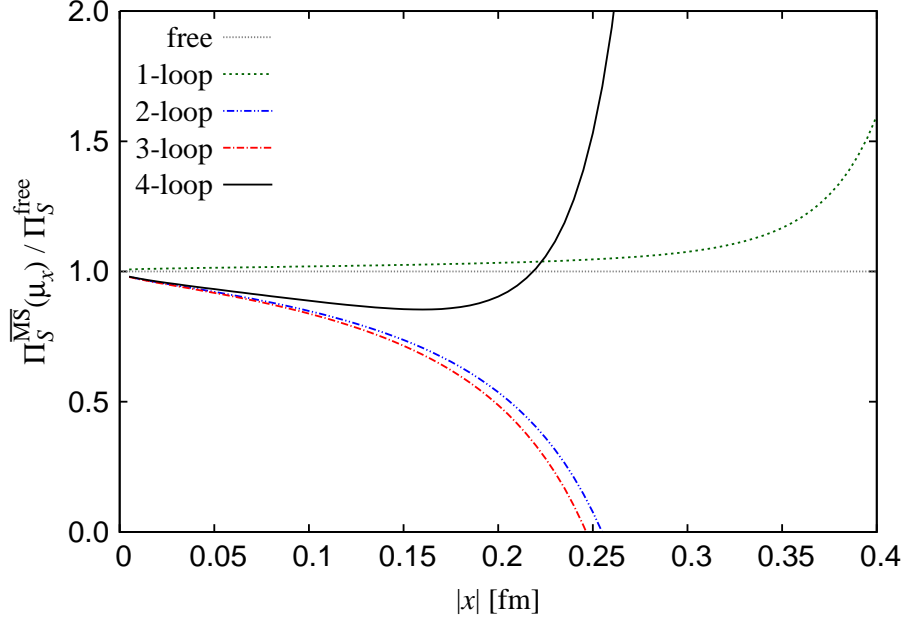


FIG. 5. Scalar correlator renormalized at μ_x in $\overline{\text{MS}}$ scheme for $n_f = 3$. The results at $\mu_x^* = \mu'_x = \mu_x$ truncated at a_s^0 (fine-dotted), a_s (dotted), a_s^2 (dashed double-dotted), a_s^3 (dashed dotted), and a_s^4 (solid) are plotted.

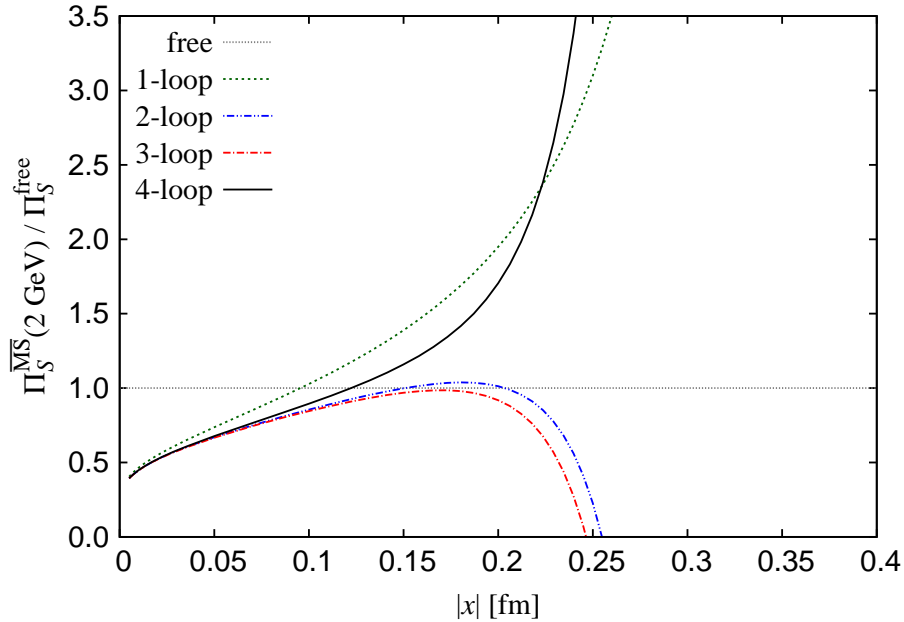


FIG. 6. Scalar correlator renormalized at 2 GeV in $\overline{\text{MS}}$ scheme for $n_f = 3$, which is calculated from the perturbative series at $\mu_x^* = \mu'_x = \mu_x$ and the scale evolution. The results truncated at a_s^0 (fine-dotted), a_s (dotted), a_s^2 (dashed double-dotted), a_s^3 (dashed dotted), and a_s^4 (solid) are plotted.

The scalar channel also shows poor convergence. The BLM scale is not directly applicable for scale dependent quantities. In fact, the BLM scale of the scalar correlator renormalized at μ_x is unstable, *i.e.* $\mu_x^{\text{BLM}} \simeq 8.8\mu_x$ for $\Pi_S^{\overline{\text{MS}}}(\tilde{\mu}_x; x)$ while $\mu_x^{\text{BLM}} \simeq 4 \times 10^3 \mu_x$ for $\Pi_S^{\overline{\text{MS}}}(\mu_x; x)$.

Since the purpose of this work is to determine the renormalization constant at 2 GeV in the $\overline{\text{MS}}$ scheme, we perform the scale evolution of the scalar correlator (12) from μ'_x to 2 GeV by a numerical integral of the mass anomalous dimension [13, 14]. Figure 6 shows the scalar correlator calculated from the perturbative series at $\mu_x^* = \mu'_x = \mu_x$ and the scale evolution with $n_f = 3$. This calculation is convergent only below $|x| \sim 0.06$ fm.

Although the scalar correlator $\Pi_S^{\overline{\text{MS}}}(2 \text{ GeV}; x)$ after the scale evolution has to be independent of both the scales μ_x^* and μ'_x , finite order calculations may depend on them. Figure 7 shows the dependences on μ_x^* and μ'_x of the four-loop results with $n_f = 3$ at four representative distances renormalized at 2 GeV in the $\overline{\text{MS}}$ scheme. To choose optimal values of μ_x^* and μ'_x , we focus on the region with mild dependence of the correlator. We choose the optimal values of $\mu'_x (= \mu_x^{\prime \text{opt}})$ as indicated by the dashed lines in Fig. 7. On these lines, the correlator depends on μ_x^* mildly and the dependence on μ'_x is also relatively small. Numerically, the choice is

$$\mu_x^{\prime \text{opt}} = e^{0.8} \mu_x \simeq \frac{2.2}{x}. \quad (13)$$

The detailed dependence of the scalar correlator on μ_x^* at $\mu'_x = \mu_x^{\prime \text{opt}}$ is shown in Fig. 8 for several distances in 0.2–0.46 fm, in which we determine the renormalization factor of the scalar operator. These figures show results at each loop order up to the four-loop level. We then choose the optimal value $\mu_x^{*, \text{opt}}$ of the scale μ_x^* as the value which minimizes the dependence on μ_x^* ,

$$\mu_x^{*, \text{opt}} = e^{1.05} \mu_x \simeq \frac{2.9}{x}. \quad (14)$$

We estimate the uncertainty by varying μ_x^* in a region including $\mu_x^{*, \text{opt}}$ in the middle as we did for the vector channel. Since the coupling constant blows up as μ_x^* approaches Λ_{QCD} , we need to avoid too small μ_x^* . Therefore, our choice is $[\frac{1}{1.6}\mu_x^{*, \text{opt}}, 1.6\mu_x^{*, \text{opt}}]$ in order not to use the coupling constant at the scale smaller than 0.75 GeV. The region is shown by the gray band in Fig. 8.

Setting μ'_x and μ_x^* by (13) and (14), we obtain the following numerical expansion at

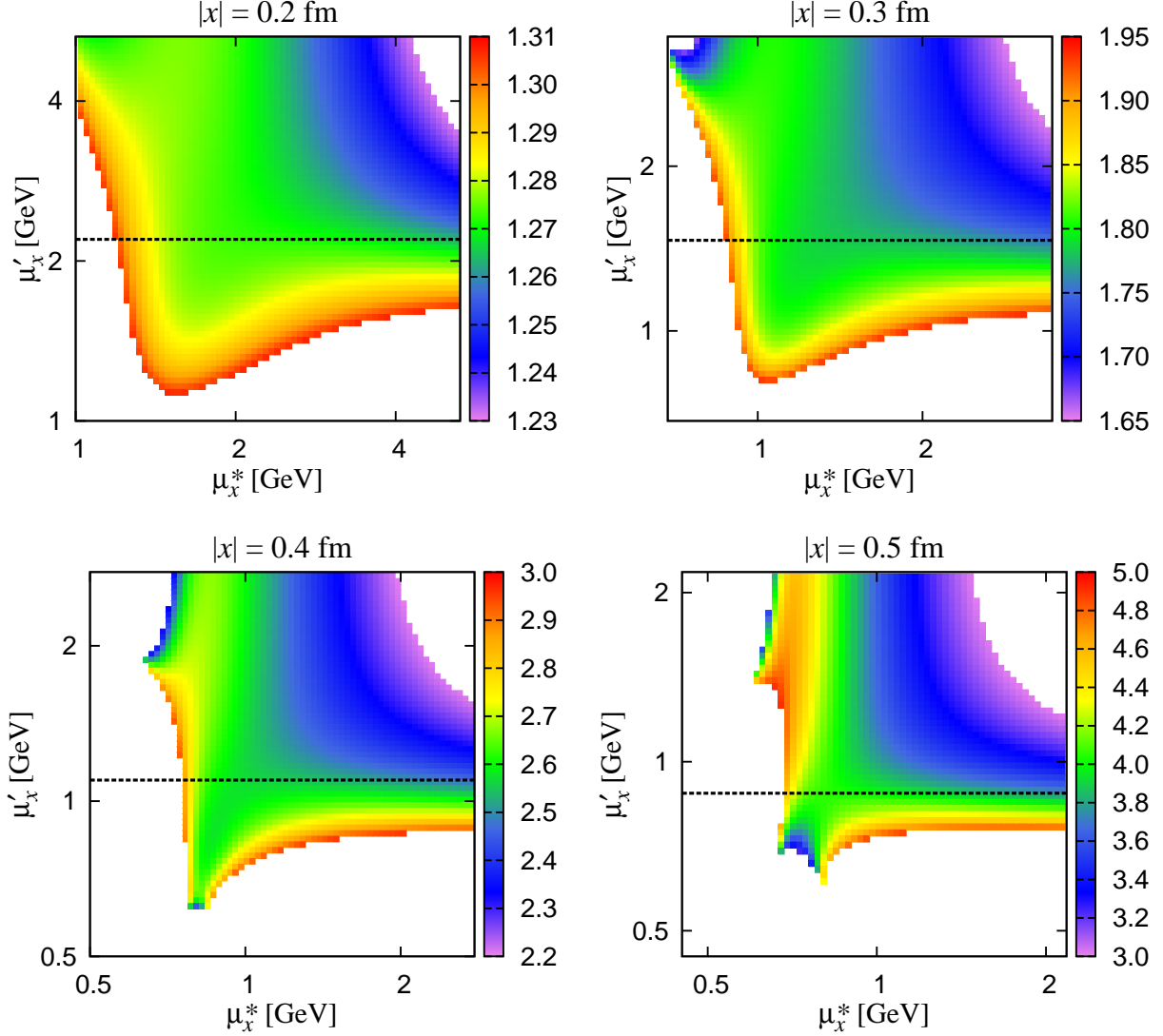


FIG. 7. $\Pi_S^{\overline{\text{MS}}}(2 \text{ GeV}; x)/\Pi_S^{\text{free}}(x)$ at the four-loop level at $n_f = 3$. The results at the specific distances 0.2 fm (top/left), 0.3 fm (top/right), 0.4 fm (bottom/left), and 0.5 fm (bottom/right) are shown as functions of μ_x^* and μ_x' . The dashed lines stand for our choice of μ_x' , where the correlator shows small sensitivity to μ_x' and μ_x^* .

$n_f = 3$,

$$\begin{aligned} \Pi_S^{\overline{\text{MS}}}(\mu_x^{\text{opt}}; x) \Big|_{n_f=3} &= \frac{3}{\pi^4 x^6} \left(1 + 3.4029 a_s(\mu_x^{*,\text{opt}}) + 9.7142 a_s(\mu_x^{*,\text{opt}})^2 \right. \\ &\quad \left. + 1.7011 a_s(\mu_x^{*,\text{opt}})^3 + 26.366 a_s(\mu_x^{*,\text{opt}})^4 + O(a_s^5) \right). \end{aligned} \quad (15)$$

The four-loop correction in this series is much smaller than that $\sim 579 a_s(\mu_x)^4$ in the perturbative series at $\mu_x^* = \mu_x$ (see Appendix A), implying that the convergence of the perturbative

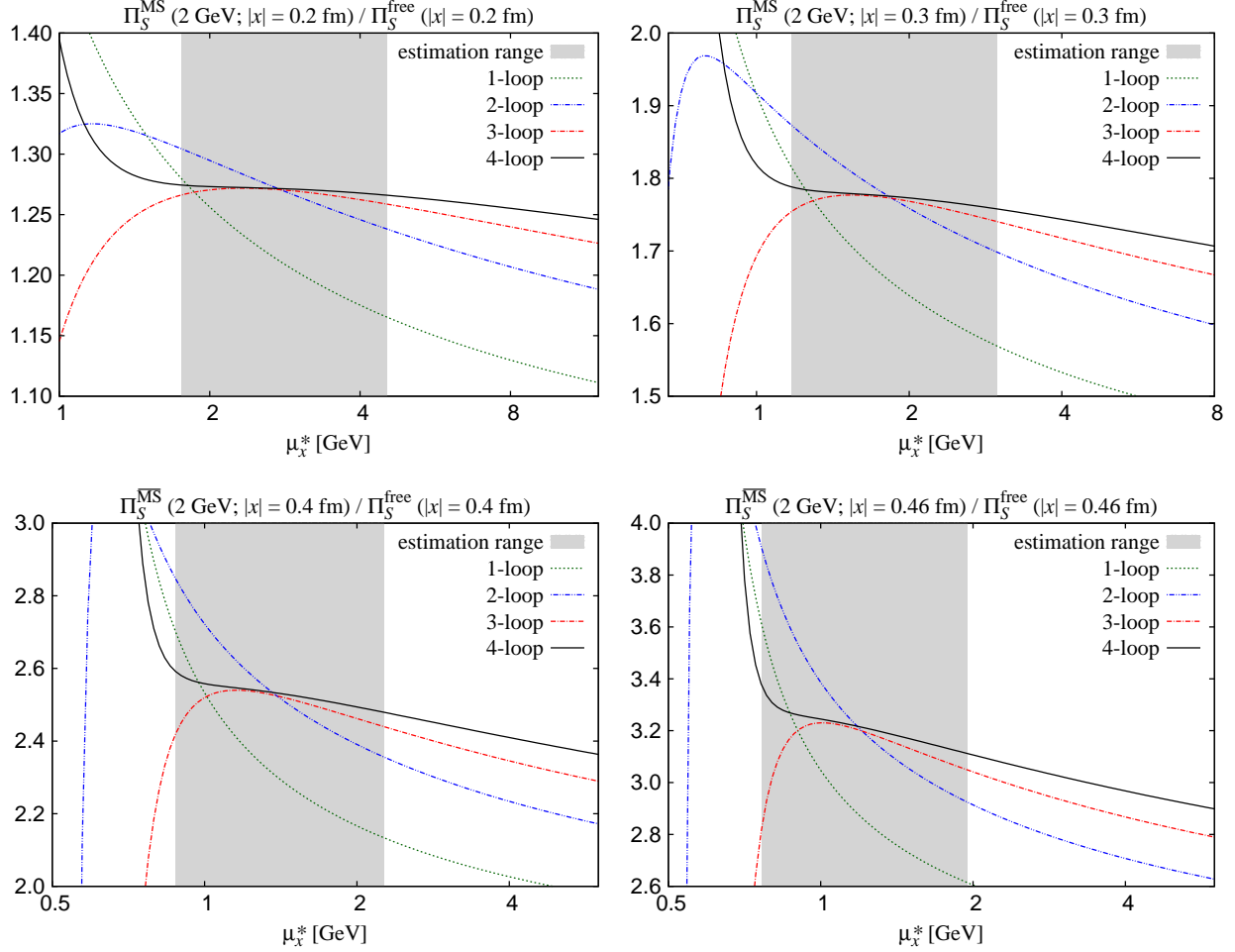


FIG. 8. Scalar correlator renormalized at 2 GeV in the $\overline{\text{MS}}$ scheme at the specific distances 0.2 fm (top/left), 0.3 fm (top/right), 0.4 fm (bottom/left), and 0.46 fm (bottom/right) as functions of μ_x^* . They are calculated at $n_f = 3$ and μ_x' is set by (13). The results truncated at a_s (dotted), a_s^2 (dashed double-dotted), a_s^3 (dashed dotted), and a_s^4 (solid) are plotted. The gray band represents the region in which we estimate the uncertainty of the perturbative calculation.

series (15) is better than that at $\mu_x^* = \mu_x$. In fact, evolving the renormalization scale of the correlator to 2 GeV, we obtain a well convergent correlator as shown in Fig. 9. The figure also shows the uncertainty of the perturbative calculation by the gray band, which is estimated by the maximum difference between the correlator at $\mu_x^* = \mu_x^{*,\text{opt}}$ and those at μ_x^* in $[\frac{1}{1.6}\mu_x^{*,\text{opt}}, 1.6\mu_x^{*,\text{opt}}]$.

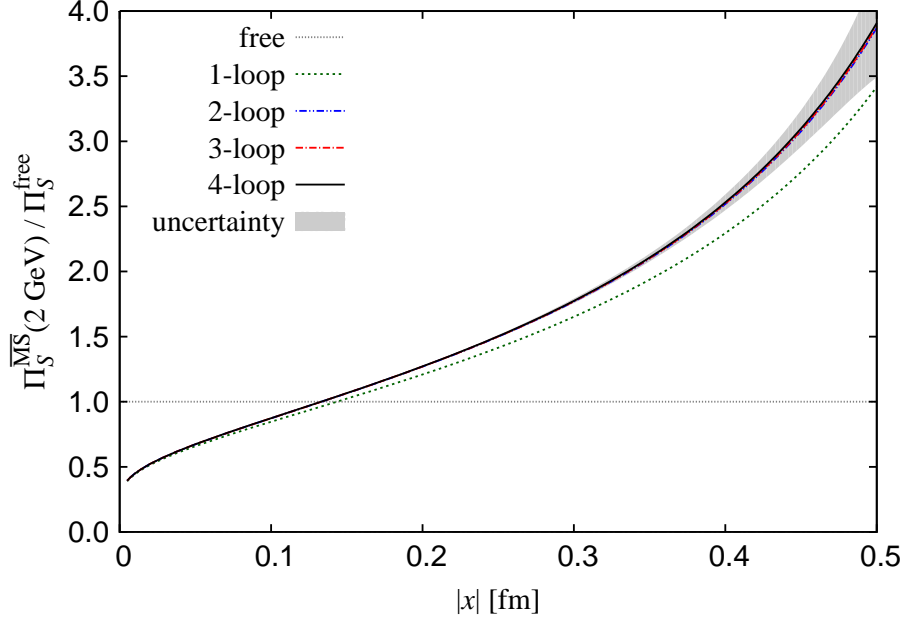


FIG. 9. Scalar correlator renormalized at 2 GeV in the $\overline{\text{MS}}$ scheme at $n_f = 3$. The scale parameters μ'_x and μ_x^* are set by (13) and (14). The results truncated at a_s^0 (fine-dotted), a_s (dotted), a_s^2 (dashed double-dotted), a_s^3 (dashed dotted), and a_s^4 (solid) are plotted. The gray region stands for the uncertainty of higher order corrections, which is estimated by the sensitivity to μ_x^* .

B. Operator Product Expansion

In the previous subsection, we discuss the correlators in perturbation theory. In the real QCD vacuum with the spontaneous breaking of chiral symmetry, however, additional terms with vacuum expectation values of operators may appear, inducing the violation of the degeneracy between the scalar and pseudoscalar, and between the vector and axial-vector channels.

In the momentum space, the Operator Product Expansion (OPE) of correlators is sketched as

$$\tilde{\Pi}_\Gamma^{\text{OPE}}(q^2) = \tilde{\Pi}_\Gamma^{\text{pert}}(q^2) + \sum_{\mathcal{O}} \tilde{c}_{\mathcal{O}}^\Gamma(q^2) q^{2-\dim \mathcal{O}} \langle \mathcal{O} \rangle, \quad (16)$$

where the first term on the RHS corresponds to the perturbative contribution including the quark mass corrections. Here \mathcal{O} denotes operators with the mass dimension four and higher,

$$\mathcal{O} \in \{m_q \bar{q}q, a_s G^2, m_q g_s \bar{q}Gq, a_s (\bar{q}q)^2, \dots\}, \quad (17)$$

and the Wilson coefficients $\tilde{c}_{\mathcal{O}}^{\Gamma}(q^2)$ do not have mass dimensions. In general, $\tilde{c}_{\mathcal{O}}^{\Gamma}$'s depend on q^2 logarithmically as $\ln(q^2/\mu^2)$ and on the quark mass as m_q^2/q^2 . These coefficients are known up to $\dim \mathcal{O} = 8$ [7, 15, 16].

The short-distance behavior of the correlators in the coordinate space is obtained by Fourier transform

$$\Pi_{\Gamma}^{\text{OPE}}(x^2) = \int \frac{d^4q}{(2\pi)^4} e^{iqx} \tilde{\Pi}_{\Gamma}^{\text{OPE}}(q^2) = \Pi_{\Gamma}^{\text{pert}}(x^2) + \sum_{\mathcal{O}} c_{\mathcal{O}}^{\Gamma}(x^2) x^{\dim \mathcal{O} - 6} \langle \mathcal{O} \rangle. \quad (18)$$

A convenient set of relations between the momentum space and the coordinate space is summarized in [17]. Using these relations, we obtain the Wilson coefficients in the coordinate space:

$$c_{m\bar{q}q}^{S/P} = \frac{1 \pm 2}{4\pi^2} + O(a_s, m_q^2 x^2), \quad c_{m\bar{q}q}^{V/A} = \frac{1 \mp 4}{2\pi^2} + O(a_s, m_q^2 x^2), \quad (19)$$

$$c_{a_s G^2}^{S/P} = \frac{1}{32\pi^2} + O(a_s, m_q^2 x^2), \quad c_{a_s G^2}^{V/A} = -\frac{1}{16\pi^2} + O(a_s, m_q^2 x^2), \quad (20)$$

$$c_{m g_s \bar{q} G q}^{S/P} = \mp \frac{1}{16\pi^2} \ln(x/x_0)^2 + O(a_s, m_q^2 x^2), \quad c_{m g_s \bar{q} G q}^{V/A} = 0, \quad (21)$$

$$c_{a_s (\bar{q}q)^2}^{S/P} = \frac{4 \pm 11}{27} \ln(x/x_0)^2 + O(a_s, m_q^2 x^2), \quad c_{a_s (\bar{q}q)^2}^{V/A} = \frac{2(2 \mp 9)}{27} \ln(x/x_0)^2 + O(a_s, m_q^2 x^2). \quad (22)$$

Here, the coefficients of the four-quark condensate $c_{a_s (\bar{q}q)^2}^{\Gamma}$ are calculated using the vacuum saturation approximation [17]. The logarithmic contributions in (21) and (22) involve dimensionful variable x_0 , which appears from divergences of the integral defining the Fourier transform and are regularization and scheme dependent.

The perturbative contribution on the RHS of (18) also includes the mass term which also violates the degeneracy of the scalar and pseudoscalar, or the vector and axial-vector channels. The massless part is already discussed in the previous subsection. The mass term contributes as

$$\Pi_{P/S}^{\text{pert}}(x^2) - \Pi_{P/S}^{\text{pert, massless}}(x^2) = -\frac{3(2 \pm 1)m_q^2}{4\pi^4 x^4} + O(\alpha_s/\pi, m_q^4/x^2), \quad (23)$$

$$\Pi_{V/A}^{\text{pert}}(x^2) - \Pi_{V/A}^{\text{pert, massless}}(x^2) = -\frac{6(1 \mp 1)m_q^2}{\pi^4 x^4} + O(\alpha_s/\pi, m_q^4/x^2). \quad (24)$$

In the renormalization condition (5), we add these mass correction terms to $\Pi_{\Gamma}^{\overline{\text{MS}}}(2 \text{ GeV}; x)$.

IV. LATTICE CALCULATION

A. Lattice Setup

TABLE I. Lattice ensembles used in this work.

β	a [fm]	$N_s^3 \times N_t \times L_s$	am_s	am_q	aM_π	N_{conf}	N_{src}		
4.17	0.0804	$32^3 \times 64 \times 12$	0.0300	0.0070	0.1263(4)	200	4		
				0.0120	0.1618(3)	200	2		
				0.0190	0.2030(3)	200	2		
		$48^3 \times 96 \times 12$	0.0400	0.0035	0.0921(1)	200	2		
					$32^3 \times 64 \times 12$	0.0070	0.1260(4)	200	4
						0.0120	0.1627(3)	200	2
			0.0190	0.2033(3)	200	2			
4.35	0.0547	$48^3 \times 96 \times 8$	0.0180	0.0042	0.0820(3)	200	2		
				0.0080	0.1127(3)	200	1		
				0.0120	0.1381(3)	200	1		
				0.0250	0.0831(4)	200	2		
				0.0080	0.1130(3)	200	1		
				0.0120	0.1387(3)	200	1		
4.47	0.0439	$64^3 \times 128 \times 8$	0.0150	0.0030	0.0632(2)	200	1		

In this work, we perform lattice simulations with 2 + 1-flavor dynamical Möbius domain-wall fermions [8, 9] with three-step stout link smearing [18] and the tree-level Symanzik improved gauge action [19]. The properties of the gauge ensembles used in this analysis are summarized in Table I. The input strange quark mass m_s is only for the sea quark, while the mass m_q of two degenerate quarks, up and down, is used for both the valence and sea quarks. The computed pion masses M_π are in the region 230–500 MeV.

For each ensemble, $N_{\text{conf}} = 200$ configurations are sampled from 10,000 molecular dynamics time. For each configuration, we calculate correlators from one or more (N_{src}) source points. We use the IroIro++ simulation code [20] for these calculations.

Considering the violation of rotational symmetry, we distinguish different lattice points that are not related by 90° rotations in the four-dimensional cubic group and average the correlators on the lattice over the lattice points that are related by 90° rotations. We then have 322 sets of different separations in the region $1 \leq (x/a)^2 \leq 100$.

B. Reduction of discretization effect

The pseudoscalar correlator $\Pi_P^{\text{lat}}(x)$ calculated non-perturbatively on the ensemble at $\beta = 4.35, (am_q, am_s) = (0.0042, 0.0180)$ is plotted in Fig. 10. This figure also shows the mean field approximation $\Pi_P^{\text{lat,mean}}(x)$ of the pseudoscalar correlator on the lattice and its asymptotic form $\Pi_P^{\text{asym,mean}}(x)$ in the long-distance limit. The mean field approximation on the lattice is calculated by a contraction of the propagators of the domain-wall fermions in the mean field theory and its long-distance limit is calculated by applying Taylor expansion (see Appendix B for more detail).

The non-perturbative lattice data are not on a smooth curve due to discretization effects. However, the similar discretization effect as seen in the free theory as well as in the mean field approximation describes the bulk of the discretization effects. We therefore improve the lattice data by applying a subtraction,

$$\Pi_\Gamma^{\text{lat}}(x) \rightarrow \Pi_\Gamma^{\text{lat}}(x) - (\Pi_\Gamma^{\text{lat,mean}}(x) - \Pi_\Gamma^{\text{asym,mean}}(x)). \quad (25)$$

As shown in Fig. 11, we obtain much smoother correlators.

Figures 12 and 13 show the pseudoscalar and vector correlators, respectively, after applying the subtraction (25). They are normalized by the continuum free correlator $\Pi_{P/V}^{\text{cont,free}}(x)$ and plotted in a linear scale. Here, we introduce a parameter θ , which is defined as an angle between the four-dimensional point x and the direction $(1, 1, 1, 1)$. In four-dimension, θ is not larger than 60° . This parameter is strongly correlated with the discretization effects as discussed in [4, 21], *i.e.* the discretization effects increase as θ increases. It is observed even after applying the subtraction (25).

As seen in Fig. 14, which is a magnification of Fig. 13 in the range $0^\circ \leq \theta \leq 30^\circ$, there are discretization effects visible already at $\theta = 30^\circ$. Although the points $(0,3,3,3)$ and $(1,1,3,4)$ are both at $(x/a)^2 = 27$ and $\theta = 30^\circ$, the values disagree beyond the statistical error. The same is observed for the data at $(0,4,4,4)$ and $(2,2,2,6)$ sharing $(x/a)^2 = 48$ and $\theta = 30^\circ$.

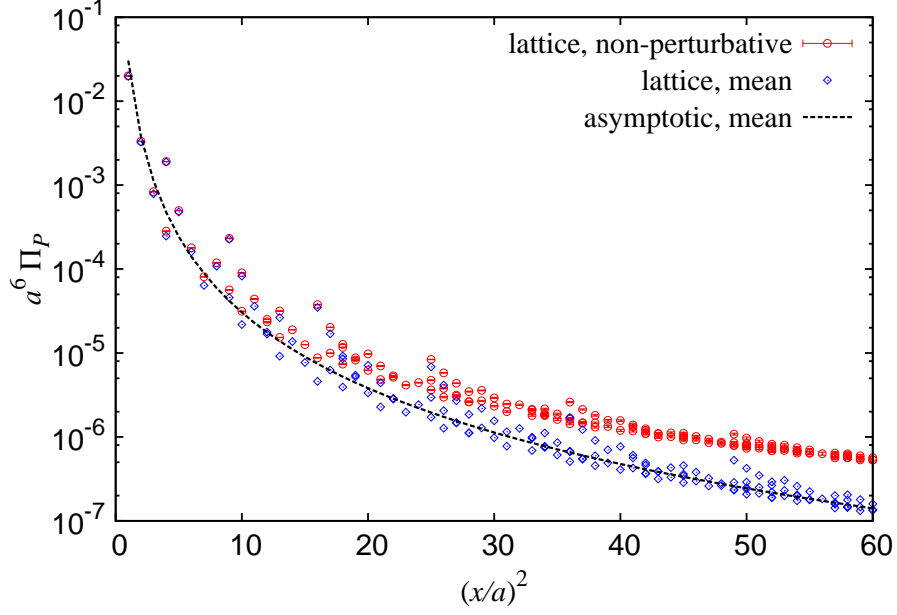


FIG. 10. Pseudoscalar correlator obtained by the lattice calculation (circles) and its mean field approximation (diamonds) at the same valence mass. The dashed curve represents the asymptotic behavior of the mean field approximation. The lattice data on the $48^3 \times 96$ at $\beta = 4.35$ and $(am_q, am_s) = (0.0042, 0.0180)$ are plotted as a representative.

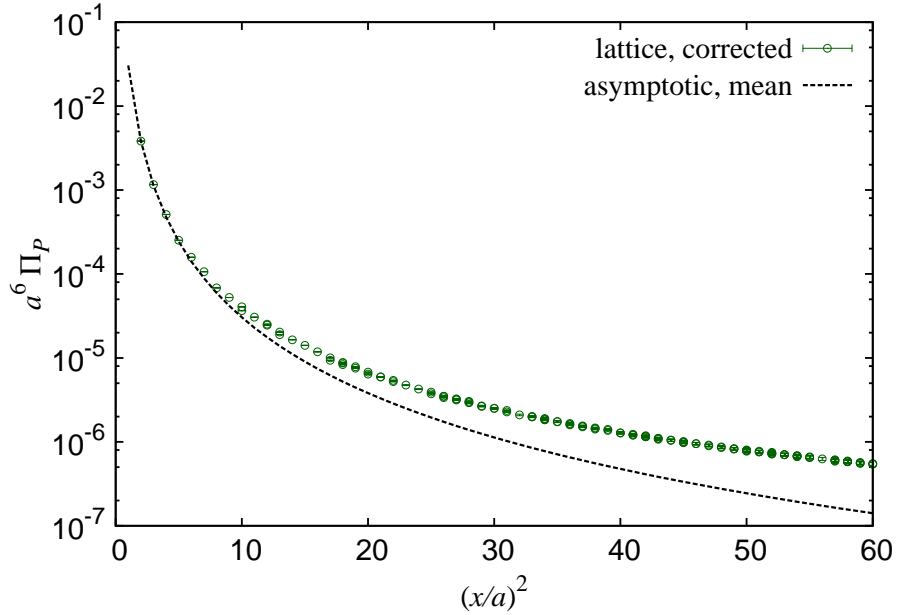


FIG. 11. Pseudoscalar correlator after applying the subtraction (25). The result on the same ensemble as in Fig. 10 is shown.

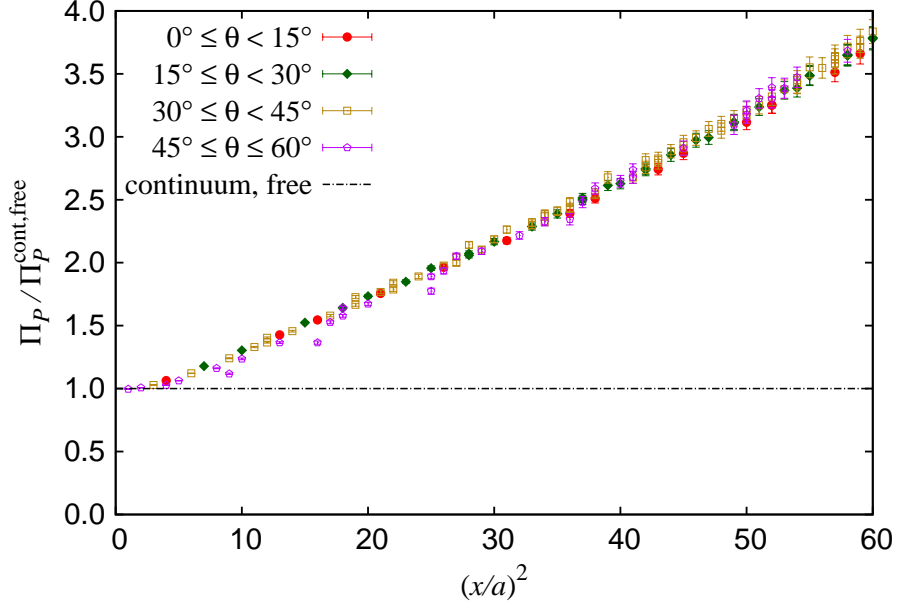


FIG. 12. Pseudoscalar correlator divided by the tree-level continuum correlator after applying the subtraction (25). The data in $0^\circ \leq \theta < 15^\circ$ (circles), $15^\circ \leq \theta < 30^\circ$ (diamonds), $30^\circ \leq \theta < 45^\circ$ (squares), and $45^\circ \leq \theta \leq 60^\circ$ (pentagons) are separately plotted. The result on the same ensemble as in Fig. 10 is shown.

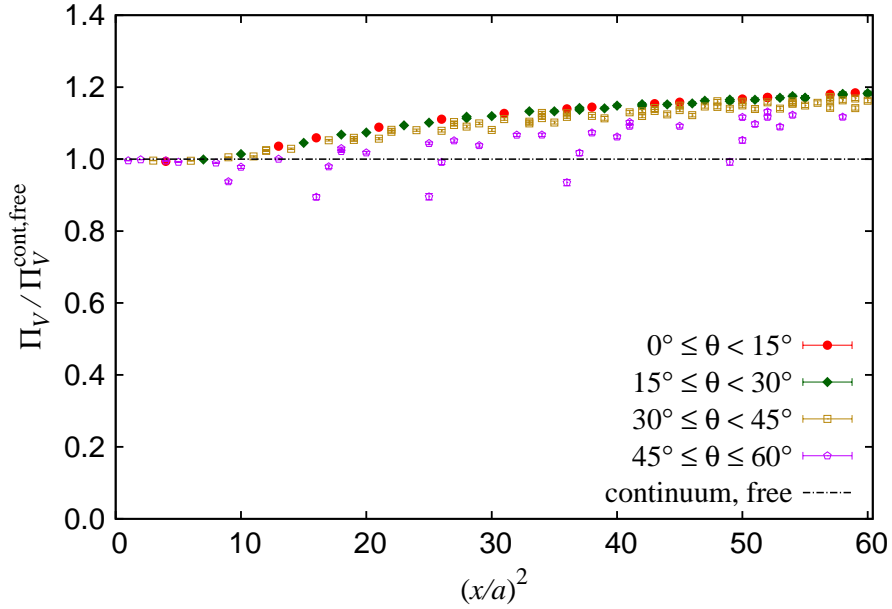


FIG. 13. Same as Fig. 12 but for the vector channel.

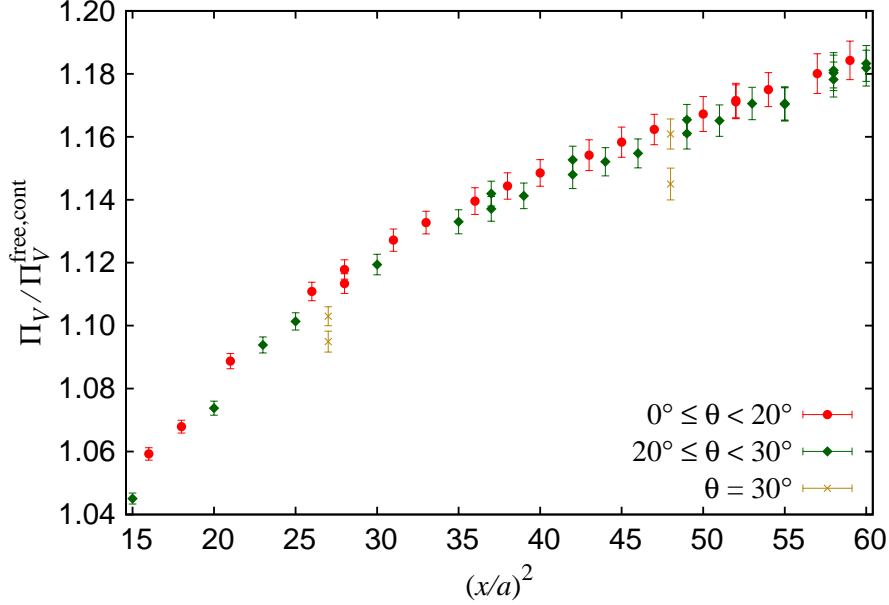


FIG. 14. Detailed view of Fig. 13. The Data in $0^\circ \leq \theta < 20^\circ$ (circles), $20^\circ \leq \theta < 30^\circ$ (diamonds), and at $\theta = 30^\circ$ (crosses) are separately plotted. Data at $\theta > 30^\circ$ are omitted.

The similar situation occurs more frequently for $\theta > 30^\circ$. Namely, the data in the region $\theta \geq 30^\circ$ cannot be simply parametrized by any functions of θ , and we therefore omit them in the analysis. Figure 14 also indicates that the lattice data at $\theta < 30^\circ$ may slightly depend on θ . For the determination of the renormalization factor in the next section, we separately treat the discretization effects at $\theta < 20^\circ$ and at $\theta \geq 20^\circ$.

C. Subtraction of finite volume effect

Point-to-point correlators may contain finite volume effect, which relates correlators $\Pi_\Gamma^{L^3 \times T}(x)$ in a finite volume with periodic boundaries to those $\Pi_\Gamma^\infty(x)$ in the infinite volume as

$$\Pi_\Gamma^{L^3 \times T}(x) = \Pi_\Gamma^\infty(x) + \sum_{x_0} \Pi_\Gamma^\infty(x - x_0), \quad (26)$$

where the sum over x_0 runs over

$$x_0 \in \{(\pm L, 0, 0, 0), (0, \pm L, 0, 0), (0, 0, \pm L, 0), (0, 0, 0, \pm T), (\pm L, \pm L, 0, 0), \dots\}. \quad (27)$$

Since the pseudoscalar correlator is expected to contain large finite volume effects due to the pion pole, we focus on this channel. The second term on the RHS of (26) is then

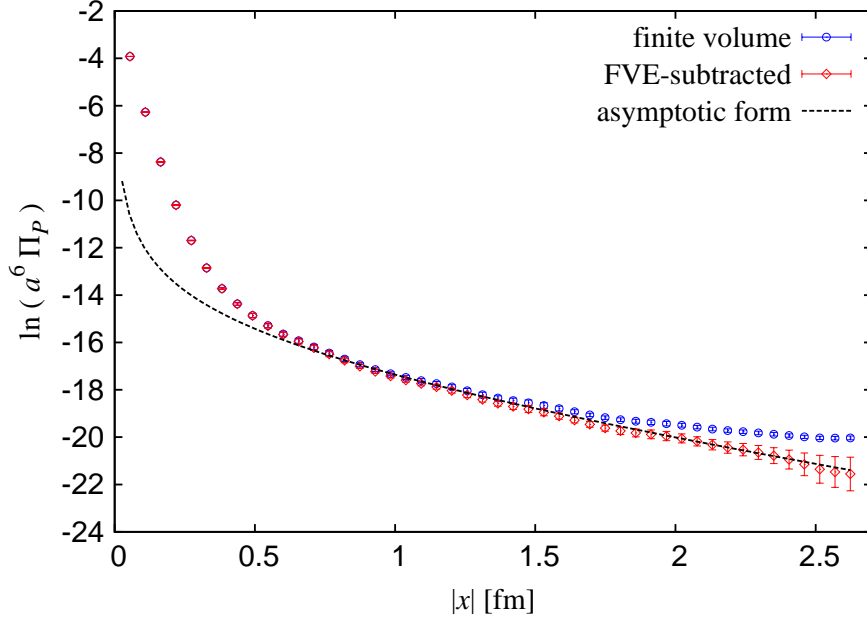


FIG. 15. Pseudoscalar correlator in the time-direction ($|x| = t$) before (circles) and after (diamonds) applying the subtraction (28). Dashed curve corresponds to the asymptotic form obtained by analyzing the zero momentum correlator. Data on the same ensemble as in Fig. 10 are plotted.

dominated by the contribution of pion, which is well approximated using the modified Bessel function K_1 . We apply the subtraction

$$\Pi_P^\infty(x) = \Pi_P^{L^3 \times T}(x) - \frac{z_0 M_\pi^2}{2\pi^2} \sum_{x_0} \frac{K_1(M_\pi |x - x_0|)}{|x - x_0|}, \quad (28)$$

where M_π and z_0 are extracted from the asymptotic form of the zero-momentum correlator, $\int d^3x \Pi_P(\vec{x}, t) \rightarrow z_0 e^{-M_\pi t}$.

Figure 15 shows the pseudoscalar correlator before and after applying the subtraction (28) of the finite volume effects. The correlators only on the time axis ($\vec{0}, t(=|x|)$) are plotted. We observe that the correlator after applying the subtraction (28) becomes consistent with the asymptotic form (dashed curve) at long distances.

From Fig. 15, we find that the finite volume effects are significant at $x \gtrsim 1$ fm. In Fig. 16, we compare $\Pi_P(x)/\Pi_P^{\text{free}}(x)$ before and after the subtraction (28) in the short distances $x \lesssim 0.5$ fm and find that the magnitude of the finite volume effect in the pseudoscalar correlator at the short distances is less than 20% of the statistical errors. Since the finite volume effects are already small in the pseudoscalar correlator, those in other channels

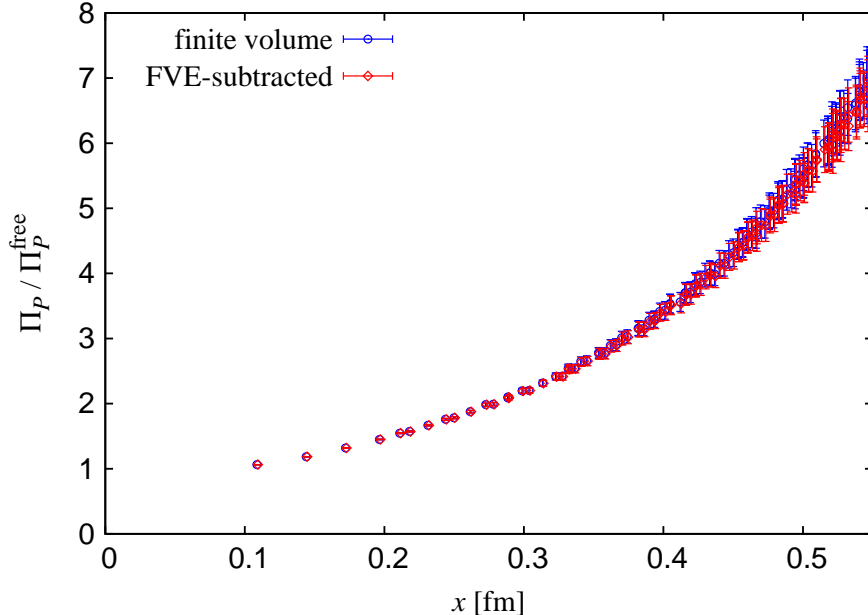


FIG. 16. Pseudoscalar correlator before (circles) and after (diamonds) applying the subtraction (28). Data on the same ensemble as in Fig. 10 are plotted.

are expected to be negligible. In this work, we apply the subtraction (28) only for the pseudoscalar channel.

V. DETERMINATION OF RENORMALIZATION CONSTANTS

A. Determination of Z_V

With domain-wall fermions that precisely satisfies the Ginsparg-Wilson relation, the identity $Z_V^{\overline{\text{MS}}/\text{lat}}(a) = Z_A^{\overline{\text{MS}}/\text{lat}}(a)$ is valid. In the analysis of $Z_V^{\overline{\text{MS}}/\text{lat}}(a)$, the renormalization scale 2 GeV can be omitted because the current conservation ensures its scale independence.

Figure 17 shows x -dependence of $\tilde{Z}_V^{\overline{\text{MS}}/\text{lat}}(a; x)$ and $\tilde{Z}_A^{\overline{\text{MS}}/\text{lat}}(a; x)$, which are defined by (5), at three input masses and $\beta = 4.35$, $am_s = 0.0180$. For $|x| < 0.2$ fm, the results increase toward the short-distance regime due to the remnant discretization effects as discussed later. For $|x| > 0.25$ fm, there is a significant splitting between the vector and axial-vector channels due to the non-perturbative effects.

The leading non-perturbative effect is described by OPE. According to the discussion in Section IIIB, the coefficients $c_{4,\bar{q}q}^V$ and $c_{4,\bar{q}q}^A$ in the OPE of the vector and axial-vector

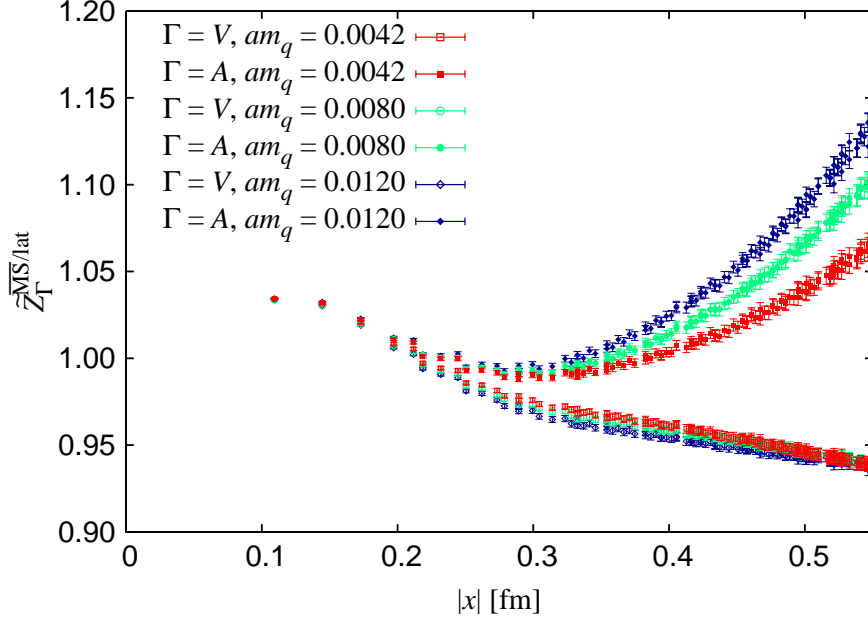


FIG. 17. $\tilde{Z}_V^{\overline{\text{MS}}/\text{lat}}(a; x)$ (open points) and $\tilde{Z}_A^{\overline{\text{MS}}/\text{lat}}(a; x)$ (filled points) calculated by (5) at the three input masses $am_q = 0.0042$ (squares), 0.080 (circles), 0.0120 (diamonds) and $\beta = 4.35, am_s = 0.0180$.

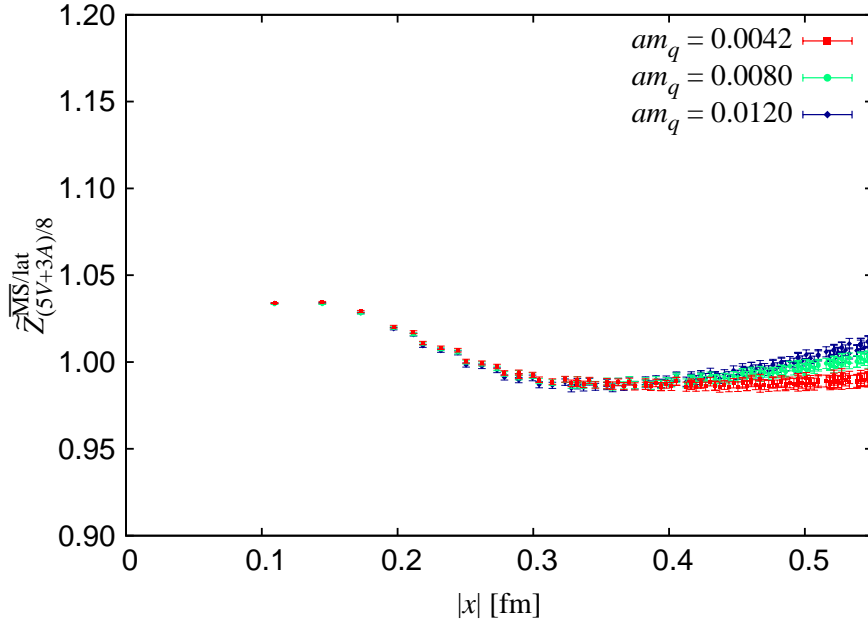


FIG. 18. $\tilde{Z}_{(5V+3A)/8}^{\overline{\text{MS}}/\text{lat}}(a; x)$ defined by (30). The results on the same ensembles as in Fig. 17 are shown.

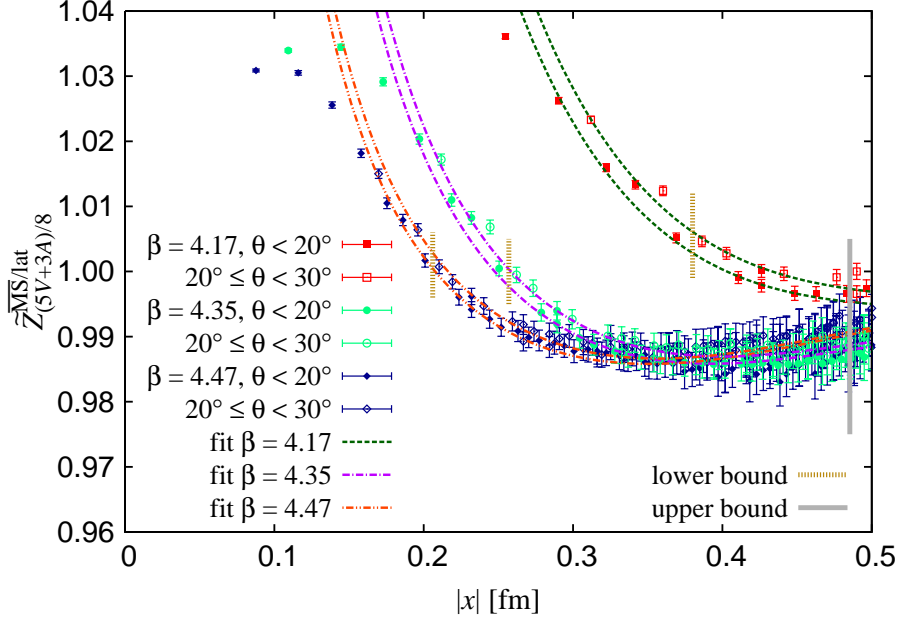


FIG. 19. $\tilde{Z}_{(5V+3A)/8}^{\overline{\text{MS}}/\text{lat}}(a; x)$ at the three of β with $M_\pi \sim 300$ MeV. For each β , the results at smaller am_s is plotted. The data at $\theta < 20^\circ$ (filled points) and $20^\circ \leq \theta < 30^\circ$ (open points) are separately plotted. The fit results for both $\theta < 20^\circ$ and $20^\circ \leq \theta < 30^\circ$ are also plotted by the curves.

correlators,

$$\Pi_{V/A}(x) = \frac{c_0}{x^6} + \frac{c_{4,\bar{q}q}^{V/A} m_q \langle \bar{q}q \rangle + c_{4,G}^{V/A} \langle GG \rangle}{x^2} + \dots, \quad (29)$$

satisfy $c_{4,\bar{q}q}^V / c_{4,\bar{q}q}^A = -3/5$ at tree level. The combination $\frac{1}{8}(5\Pi_V + 3\Pi_A)$ is therefore expected to cancel the leading contribution of the chiral condensate. Therefore we analyze

$$\tilde{Z}_{(5V+3A)/8}^{\overline{\text{MS}}/\text{lat}}(a; x) = \sqrt{\frac{\Pi_V^{\overline{\text{MS}}}(a; x)}{\frac{1}{8}(5\Pi_V^{\text{lat}}(a; x) + 3\Pi_A^{\text{lat}}(a; x))}}, \quad (30)$$

to extract the renormalization constant suppressing the non-perturbative effect. We find that both the $|x|$ -dependence and the mass dependence are dramatically reduced as shown in Fig. 18. Although there is no mass dependence remaining for $\tilde{Z}_{(3V+5A)/8}^{\overline{\text{MS}}/\text{lat}}(a; x)$ in the OPE for the operators of dimension four, the data still have sizable mass dependence for $|x| > 0.4$ fm. This mass dependence may originate from higher dimensional operators including $m_q^2 \langle GG \rangle$ and $m_q^3 \langle \bar{q}q \rangle$. Another mass-independent operator $\langle \bar{q}q\bar{q}q \rangle$ with the same mass dimension should also be considered.

Figure 19 shows $\tilde{Z}_{(5V+3A)/8}^{\overline{\text{MS}}/\text{lat}}(a; x)$ obtained at three β values with approximately matched quark masses. The position where $\tilde{Z}_{(5V+3A)/8}^{\overline{\text{MS}}/\text{lat}}(a; x)$ starts deviating from a constant toward

short distances moves as the lattice spacing is reduced, indicating that this deviation is due to the discretization effects. The most significant discretization effect is of $O(a^2)$ which appears as $(a/x)^2$. Since we already subtract discretization effects at the tree-level, $\alpha_s(\beta)(a/x)^2$ is the leading remaining discretization effects. As discussed in Section IV B, we discard the data in $\theta \geq 30^\circ$ and parametrize the discretization effects in $0^\circ \leq \theta < 20^\circ$ and in $20^\circ \leq \theta < 30^\circ$ separately as described below.

We determine $Z_V^{\overline{\text{MS}}/\text{lat}}$ by a simultaneous fit of the data on all ensembles using the fit function

$$\begin{aligned} \tilde{Z}_{(5V+3A)/8}^{\overline{\text{MS}}/\text{lat}}(a; x) = & Z_V^{\overline{\text{MS}}/\text{lat}}(\beta) \\ & + C_{-2}(\theta)\alpha_s(\beta)(a/x)^2 + C_{4,G}x^4 + (C_{6,q} + C_{6,mG}m_q^2 + C_{6,mq}m_q^3)x^6, \end{aligned} \quad (31)$$

with nine free parameters $Z_V^{\overline{\text{MS}}/\text{lat}}$ (4.17), $Z_V^{\overline{\text{MS}}/\text{lat}}$ (4.35), $Z_V^{\overline{\text{MS}}/\text{lat}}$ (4.47), $C_{-2}(\theta < 20^\circ)$, $C_{-2}(20^\circ \leq \theta < 30^\circ)$, $C_{4,G}$, $C_{6,q}$, $C_{6,mG}$, and $C_{6,mq}$. Here, the last four parameters correspond to the contribution of $\langle a_s GG \rangle$, $\langle \bar{q}q\bar{q}q \rangle$, $m_q^2 \langle GG \rangle$, and $m_q^3 \langle \bar{q}q \rangle$, respectively. In this analysis, we neglect the $O(a_s)$ correction to the Wilson coefficients of these operators. The terms of $O(x^6)$ involve the logarithmic dependence $\ln(x/x_0)^2$ as discussed in Section III B. Here we do not consider this effect because $\ln(x/x_0)^2$ is roughly constant in the fit range and their effects cannot be identified. The fit results are shown in Fig. 19 by the curves. Here, both the results for $\theta < 20^\circ$ and $20^\circ \leq \theta < 30^\circ$ are plotted.

In Table II, the results for $Z_V^{\overline{\text{MS}}/\text{lat}}$ are summarized with the errors from various sources. The first error is the statistical error. The second represents the discretization error. The central value is the fit result with a lower bound $(x_{\text{low}}/a)^2 = 23$, which is shown in Fig. 19. and the second error is estimated by moving the lower bound in the region $19 \leq (x_{\text{low}}/a)^2 \leq$

TABLE II. Result for the renormalization factor $Z_V^{\overline{\text{MS}}/\text{lat}}(a)$ of the vector channel.

β	$Z_V^{\overline{\text{MS}}/\text{lat}}(a)$	Errors			
		Stat.	Disc.	μ_x^*	Λ_{QCD}
4.17	0.9553	(53)	(74)	(8)	(5)
4.35	0.9636	(34)	(46)	(7)	(4)
4.47	0.9699	(26)	(38)	(6)	(4)

27 and taking the largest difference from the central value. The third is an estimate of the uncertainty of the higher order corrections of the perturbative expansion as discussed in Section III A. The central value is calculated with $\mu_x^{*,\text{opt}}$ in (10) and the uncertainty is estimated by the maximum difference of results with μ_x^* in the region $[\frac{1}{2}\mu_x^{*,\text{opt}}, 2\mu_x^{*,\text{opt}}]$. The last error is from the uncertainty of Λ_{QCD} or of the strong coupling constant. We use the value $\Lambda_{\text{QCD}}^{\overline{\text{MS}},n_f=3} = 340(8)$ MeV reported by Particle Data Group [22]. The uncertainty of the lattice spacing does not significantly affect the results. The upper bound of the fit range is fixed to 0.485 fm.

The fit result for other parameters reads

$$\begin{aligned}
C_{-2}(\theta < 20^\circ) &= 14.0(1.2)(2.0)(1)(1), & C_{-2}(20^\circ \leq \theta < 30^\circ) &= 15.1(1.1)(2.2)(1)(-), \\
C_{4,G} &= 0.564(190)(187)(99)(14) \text{ fm}^{-4}, & C_{6,q} &= -0.109(61)(56)(4)(3) \text{ fm}^{-6}, \\
C_{6,mG} &= -19.8(31.5)(5)(3)(1) \text{ fm}^{-4}, & C_{6,mq} &= 192(125)(2)(2)(1) \text{ fm}^{-3}.
\end{aligned}$$

The consistency of this analysis can be checked by evaluating the gluon condensate from the fit result. Using (20) and the fit result $C_{4,G}$, we obtain $\langle(\alpha_s/\pi)GG\rangle = 0.017(6)(6)(3)(-)$ GeV⁴ at the lowest order of α_s/π . The errors are estimated in the similar manner. This result is in good agreement with known values, *e.g.* $\langle(\alpha_s/\pi)GG\rangle = 0.012$ GeV⁴ from the sum rule for charmonium [7] and $\langle(\alpha_s/\pi)GG\rangle = 0.006(12)$ GeV⁴ from the spectral functions of hadronic τ decays [23].

B. Determination of Z_S

The domain-wall fermion also guarantees the agreement of the renormalization constants of the scalar $Z_S^{\overline{\text{MS}}/\text{lat}}(a)$ and pseudoscalar $Z_P^{\overline{\text{MS}}/\text{lat}}(a)$ densities. The determination of $Z_S^{\overline{\text{MS}}/\text{lat}}(a)$ and $Z_P^{\overline{\text{MS}}/\text{lat}}(a)$ may be more complicated due to the instanton-induced 't Hooft interactions [24, 25], which affect the scalar and pseudoscalar correlators significantly and are not described by OPE. Since the instanton effects to the scalar and pseudoscalar correlators are the same magnitude with an opposite sign, the naïve average $\frac{1}{2}(\Pi_S(x) + \Pi_P(x))$ may cancel such effects and could be well explained by OPE. The average contains the contribution of the chiral condensate in OPE, which we try to cancel by using the difference

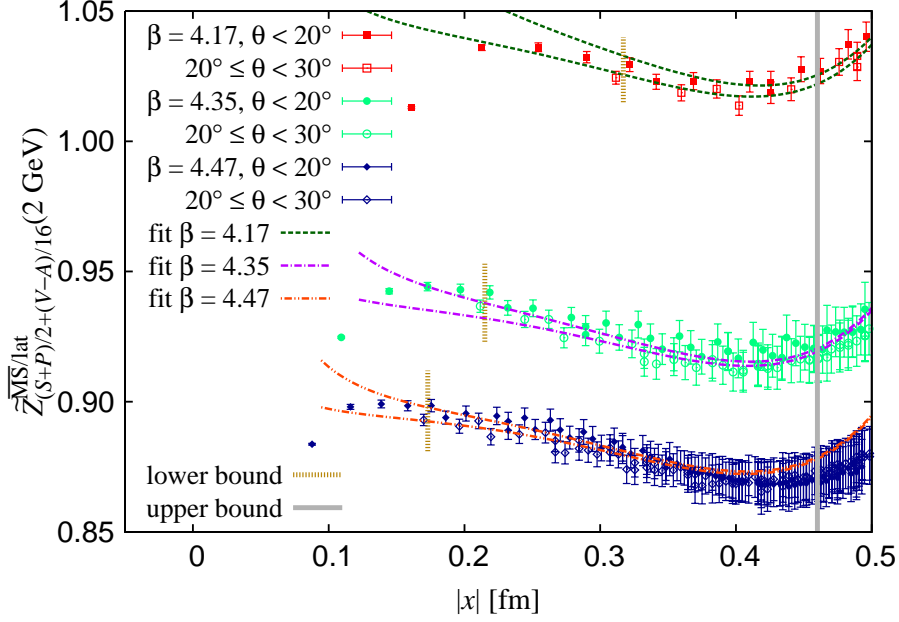


FIG. 20. Same as Fig. 19 but for $\tilde{Z}_{(S+P)/2+(V-A)/16}^{\overline{\text{MS}}/\text{lat}}(2 \text{ GeV}, a; x)$

between the vector and axial-vector correlators. Namely, we analyze

$$\begin{aligned} & \tilde{Z}_{(S+P)/2+(V-A)/16}^{\overline{\text{MS}}/\text{lat}}(2 \text{ GeV}, a; x) \\ &= \sqrt{\frac{\Pi_S^{\overline{\text{MS}}}(2 \text{ GeV}; x)}{\frac{1}{2}(\Pi_S^{\text{lat}}(a; x) + \Pi_P^{\text{lat}}(a; x)) + \frac{1}{16}(\Pi_V^{\text{lat}}(a; x) - \Pi_A^{\text{lat}}(a; x))}}, \end{aligned} \quad (32)$$

whose OPE does not depend on the chiral condensate $m_q \langle \bar{q}q \rangle x^4$ at the tree-level. Since we neglect the $O(a_s)$ correction to the Wilson coefficients in this analysis, we omit the renormalization factor for $\Pi_V^{\text{lat}}(a; x) - \Pi_A^{\text{lat}}(a; x)$.

We implement the simultaneous fit to the data of (32) with the same function as (31).

TABLE III. Result for the renormalization factor $Z_S^{\overline{\text{MS}}/\text{lat}}(2 \text{ GeV}, a)$ of the scalar channel.

β	$Z_S^{\overline{\text{MS}}/\text{lat}}(2 \text{ GeV}, a)$	Errors			
		Stat.	Disc.	μ_x^*	Λ_{QCD}
4.17	1.0372	(93)	(77)	(57)	(58)
4.35	0.9342	(57)	(43)	(37)	(34)
4.47	0.8926	(41)	(35)	(30)	(25)

The results are summarized in Table III. The error estimation is done in the similar manner as that for the vector channel. We choose the lower bound of the fit range as $(x_{\text{low}}/a)^2 = 16$ for the central value and estimate the second error by changing x_{low} in the region $12 \leq (x_{\text{low}}/a)^2 \leq 20$. The central $\mu_x^* = \mu_x^{*,\text{opt}}$ is given by (14) and the third error is estimated by varying μ_x^* in the region $[\frac{1}{1.6}\mu_x^{*,\text{opt}}, 1.6\mu_x^{*,\text{opt}}]$. The upper bound of the fit range is fixed to 0.460 fm. The fit result is shown in Fig. 20 for the same ensembles as in Fig. 19.

The fit result for other parameters reads

$$\begin{aligned}
C_{-2}(\theta < 20^\circ) &= 2.25(1.37)(1.81)(58)(77), & C_{-2}(20^\circ \leq \theta < 30^\circ) &= 0.522(1.39)(1.72)(60)(80), \\
C_{4,G} &= -2.27(52)(25)(23)(33) \text{ fm}^{-4}, & C_{6,q} &= 7.71(52)(1.08)(2.19)(45) \text{ fm}^{-6}, \\
C_{6,mG} &= 212(156)(4)(3)(2) \text{ fm}^{-4}, & C_{6,mq} &= -432(622)(18)(7)(3) \text{ fm}^{-3}.
\end{aligned}$$

VI. CONCLUSION

We have determined the renormalization factors $Z_V^{\overline{\text{MS}}/\text{lat}}(a)$, $Z_S^{\overline{\text{MS}}/\text{lat}}(2 \text{ GeV}, a)$ of the flavor non-singlet quark bilinear operators composed of Möbius domain-wall fermions by analyzing correlation functions in the coordinate space. This method enables us to renormalize in a fully gauge invariant manner and to implement the perturbative matching up to the four-loop level. We impose the direct renormalization condition onto the $\overline{\text{MS}}$ scheme without introducing any intermediate renormalization schemes.

Although the complicated analysis is required to eliminate discretization effects that are significant at short distances, the results obtained in this work and their accuracy demonstrate the use of the X-space method. It is already at a competing level with the RI/MOM methods, and we expect it becomes more so in the future as the lattice spacing is reduced, because the perturbative error would become the dominant source in such situation.

Direct applications of our results are the calculation of meson decay constants and quark masses. Some preliminary results are found in [26]. The (pseudo)scalar renormalization factor is also necessary for the determination of the chiral condensate, which characterizes the spontaneous broken chiral symmetry in QCD. We can extract this important quantity from the same set of correlators as we analyzed in this work, through the axial Ward-Takahashi identity. Such analysis will be presented in a forthcoming paper. The same quantity can be obtained with a completely different method, *i.e.* from the eigenvalue density of the Dirac operator through the Banks-Casher relation. A preliminary analysis on our ensembles was

presented in [27].

Current correlators at short distances contain more information of QCD. They are complicated mixture of excited states of hadrons, but at the same time they can be analyzed using perturbation theory. For the analysis of the intermediate region between perturbative and non-perturbative regimes, the lattice data may provide useful information, that can be used to study the range of application of perturbative expansion in perturbative QCD for instance. The work in such directions are in progress.

ACKNOWLEDGMENTS

Numerical simulations are performed on Hitachi SR 16000 and IBM System Blue Gene Solution at KEK under a support of its Large Scale Simulation Program (No. 13/14-04, 14/15-10). We thank P. Boyle for the optimized code for BGQ. This work is supported in part by the Grant-in-Aid of the Japanese Ministry of Education (No. 25800147, 26247043, 26400259,15K05065) and by MEXT SPIRE and JICFuS.

Appendix A: Summary of perturbative coefficients

This appendix summarizes numerical coefficients of perturbative expansions of the vector and scalar correlators obtained by using the four-loop results of correlators [5], the beta function [12], and the anomalous dimension [13, 14].

For the vector channel, the perturbative coefficients C_i^V 's at $\mu_x^* = \mu_x$ and the corresponding perturbative expansion with $n_f = 3$ are

$$\begin{aligned}
C_1^V(\mu_x) &= 1, \\
C_2^V(\mu_x) &= -5.5269 + 0.34002n_f, \\
C_3^V(\mu_x) &= 10.415 - 3.2912n_f + 0.12602n_f^2, \\
C_4^V(\mu_x) &= 28.928 + 30.966n_f - 2.6652n_f^2 + 0.064007n_f^3,
\end{aligned} \tag{A1}$$

$$\begin{aligned}
\Pi_V^{\overline{\text{MS}}}(x) \Big|_{n_f=3} &= \frac{6}{\pi^4 x^6} \left(1 + a_s(\mu_x) - 4.5069a_s(\mu_x)^2 \right. \\
&\quad \left. + 1.6758a_s(\mu_x)^3 + 99.567a_s(\mu_x)^4 + O(a_s^5) \right).
\end{aligned} \tag{A2}$$

At $\mu_x^* = \tilde{\mu}_x$, C_i^V 's and the expansion are given by

$$\begin{aligned}
C_1^V(\tilde{\mu}_x) &= 1, \\
C_2^V(\tilde{\mu}_x) &= -4.8893 + 0.30137n_f, \\
C_3^V(\tilde{\mu}_x) &= 5.2517 - 2.6633n_f + 0.10124n_f^2, \\
C_4^V(\tilde{\mu}_x) &= 33.562 + 26.233n_f - 2.2001n_f^2 + 0.050863n_f^3,
\end{aligned} \tag{A3}$$

$$\begin{aligned}
\Pi_V^{\overline{\text{MS}}}(x) \Big|_{n_f=3} &= \frac{6}{\pi^4 x^6} \left(1 + a_s(\tilde{\mu}_x) - 3.9852a_s(\tilde{\mu}_x)^2 \right. \\
&\quad \left. - 1.8270a_s(\tilde{\mu}_x)^3 + 93.835a_s(\tilde{\mu}_x)^4 + O(a_s^5) \right).
\end{aligned} \tag{A4}$$

Finally, at $\mu_x^* = \tilde{\mu}_x$, C_i^V 's and the expansion are

$$\begin{aligned}
C_1^V(\mu_x^{\text{BLM}}) &= 1, \\
C_2^V(\mu_x^{\text{BLM}}) &= 0.083333, \\
C_3^V(\mu_x^{\text{BLM}}) &= -7.1191 - 1.1478n_f + 0.010414n_f^2, \\
C_4^V(\mu_x^{\text{BLM}}) &= -56.886 + 12.283n_f - 0.58326n_f^2 + 0.014075n_f^3,
\end{aligned} \tag{A5}$$

$$\begin{aligned}
\Pi_V^{\overline{\text{MS}}}(x) \Big|_{n_f=3} &= \frac{6}{\pi^4 x^6} \left(1 + a_s(\mu_x^{\text{BLM}}) + 0.083333a_s(\mu_x^{\text{BLM}})^2 \right. \\
&\quad \left. - 10.469a_s(\mu_x^{\text{BLM}})^3 - 24.907a_s(\mu_x^{\text{BLM}})^4 + O(a_s^5) \right).
\end{aligned} \tag{A6}$$

For the scalar channel, the perturbative coefficients C_i^S 's at $\mu_x^* = \mu'_x = \mu_x$ and the corresponding expansion with $n_f = 3$ are

$$\begin{aligned}
C_1^S(\mu_x, \mu_x) &= 0.20294, \\
C_2^S(\mu_x, \mu_x) &= -20.197 + 0.56314n_f, \\
C_3^S(\mu_x, \mu_x) &= 7.8854 - 7.5318n_f + 0.37635n_f^2, \\
C_4^S(\mu_x, \mu_x) &= 500.95 + 40.402n_f - 5.3403n_f^2 + 0.18479n_f^3,
\end{aligned} \tag{A7}$$

$$\begin{aligned}
\Pi_S^{\overline{\text{MS}}}(\mu_x; x) \Big|_{n_f=3} &= \frac{3}{\pi^4 x^6} \left(1 + 0.20294a_s(\mu_x) - 18.507a_s(\mu_x)^2 \right. \\
&\quad \left. - 11.323a_s(\mu_x)^3 + 579.08a_s(\mu_x)^4 + O(a_s^5) \right).
\end{aligned} \tag{A8}$$

At $\mu_x^* = \mu'_x = \tilde{\mu}_x$, C_i^S 's and the expansion are given by

$$\begin{aligned}
C_1^S(\tilde{\mu}_x, \tilde{\mu}_x) &= \frac{2}{3}, \\
C_2^S(\tilde{\mu}_x, \tilde{\mu}_x) &= -17.766 + 0.48193n_f, \\
C_3^S(\tilde{\mu}_x, \tilde{\mu}_x) &= -14.656 - 6.3172n_f + 0.32333n_f^2, \\
C_4^S(\tilde{\mu}_x, \tilde{\mu}_x) &= 450.45 + 25.502n_f - 3.8057n_f^2 + 0.14697n_f^3,
\end{aligned} \tag{A9}$$

$$\begin{aligned}
\Pi_S^{\overline{\text{MS}}}(\tilde{\mu}_x; x) \Big|_{n_f=3} &= \frac{3}{\pi^4 x^6} \left(1 + 0.66667a_s(\tilde{\mu}_x) - 16.321a_s(\tilde{\mu}_x)^2 \right. \\
&\quad \left. - 30.698a_s(\tilde{\mu}_x)^3 + 496.67a_s(\tilde{\mu}_x)^4 + O(a_s^5) \right).
\end{aligned} \tag{A10}$$

Appendix B: Mean field approximation of correlators on the lattice

Correlators in the coordinate space are given by

$$\Pi_\Gamma(x) = \langle \text{Tr} [S_F(x) \Gamma S_F(-x) \Gamma] \rangle, \tag{B1}$$

where $S_F(x)$ stands for the propagator of the Dirac field. We give the mean field approximation of the domain-wall propagator and its asymptotic form in the long-distance limit. Since the residual mass in this work is almost negligible, we consider the domain-wall propagator with the infinite size of the fifth direction $L_s \rightarrow \infty$. The four-dimensional representation $\tilde{S}_F^{\text{DW}}(q, m_q)$ of the mean field domain-wall propagator in the momentum space is [11, 28, 29]

$$\tilde{S}_F^{\text{DW}}(q, m_q)/a = \frac{-i\gamma_\mu u_0 \sin(aq_\mu) + (1 - W e^{-\alpha}) a m_q}{-1 + W e^\alpha + (1 - W e^{-\alpha})(a m_q)^2}, \tag{B2}$$

where W and α are defined by

$$W(q) = 1 - M_0 + \sum_\mu (1 - u_0 \cos(aq_\mu)), \tag{B3}$$

$$\cosh \alpha(q) = \frac{1 + W^2 + u_0^2 \sum_\mu \sin^2(aq_\mu)}{2W}, \tag{B4}$$

with M_0 and u_0 being the domain-wall mass parameter and the fourth root of the plaquette expectation value, respectively. The free propagator is reproduced by putting $u_0 = 1$.

The propagator in the coordinate space is calculated by a numerical Fourier transform in a finite box L^4 ,

$$S_F^{\text{DW}, L^4}(x, m_q) = \frac{1}{L^4} \sum_q \tilde{S}_F^{\text{DW}}(q) e^{iqx}, \tag{B5}$$

where the sum over q for the periodic boundary condition runs over

$$q \in \left\{ \frac{2\pi}{L}(k_1, k_2, k_3, k_4) \mid k_\mu = -\frac{L}{2a} + 1, -\frac{L}{2a} + 2, \dots, \frac{L}{2a} \right\}, \quad (\text{B6})$$

The mean field approximation of the propagator of a light quark in a finite box ($m_q L \lesssim 1$) involves large finite volume effects because quarks are in the deconfining phase. Since the numerical Fourier transform in sufficient large volumes is expensive, we apply a correction for the domain-wall propagator as we applied for the propagators of bosonic fields in Section IV C,

$$\begin{aligned} S_F^{\text{DW},\infty}(x, m_q) &= S_F^{\text{DW},L^4}(x, m_q) - \sum_{x_0} S_F^{\text{DW},\infty}(x - x_0, m_q) \\ &\simeq S_F^{\text{DW},L^4}(x, m_q) - \sum_{x_0} S_F^{\text{DW},\text{asym}}(x - x_0, m_q), \end{aligned} \quad (\text{B7})$$

where the sum over x_0 runs over

$$x_0 \in \{(\pm L, 0, 0, 0), (0, \pm L, 0, 0), (0, 0, \pm L, 0), (0, 0, 0, \pm L), (\pm L, \pm L, 0, 0), \dots\}, \quad (\text{B8})$$

and $S_F^{\text{DW},\text{asym}}(x)$ is the asymptotic form of the domain-wall propagator in the long-distance limit in the infinite volume, which is calculated as follows.

The domain-wall propagator in the low-momentum region is calculated by expanding (B2) at $aq \simeq 0$,

$$\tilde{S}_F^{\text{DW}}(q, m_q) \xrightarrow{aq \rightarrow 0} (1 - \delta^2) \frac{-i u_0 \not{q} + m'_q}{u_0^2 q^2 + m_q'^2} + O(\delta^4), \quad (\text{B9})$$

with

$$\delta = 1 - M_0 + 4(1 - u_0), \quad (\text{B10})$$

$$m'_q = (1 - \delta^2)m_q. \quad (\text{B11})$$

The Fourier transform of this propagator in the infinite volume gives an asymptotic form in the long-distance limit of the domain-wall propagator,

$$S_F^{\text{DW},\text{asym}}(x, m_q) = \frac{1 - \delta^2}{u_0^4} S_F^{\text{cont}}(x/u_0, m'_q) + O(\delta^4), \quad (\text{B12})$$

where the Feynman propagator $S_F^{\text{cont}}(x, m_q)$ of a Dirac field in the continuum coordinate space is given [30] by

$$\begin{aligned} S_F^{\text{cont}}(x, m_q) &= \int \frac{d^4 q}{(2\pi)^4} e^{iqx} \frac{-i\not{q} + m_q}{q^2 + m_q^2} \\ &= \frac{m_q \not{x}}{4\pi^2 |x|^3} K_1(m_q |x|) + \frac{m_q^2 \not{x}}{8\pi^2 x^2} [K_0(m_q |x|) + K_2(m_q |x|)] + \frac{m_q^2}{4\pi^2 |x|} K_1(m_q |x|), \end{aligned} \quad (\text{B13})$$

with K_i being the modified Bessel functions.

The subtraction by the second line of (B7) cannot eliminate discretization effects of wrapping effects, *i.e.* the subtraction leaves the discretization effects

$$\sum_{x_0} (S_F^{\text{DW},\infty}(x - x_0, m_q) - S_F^{\text{DW,asym}}(x - x_0, m_q)), \quad (\text{B14})$$

which are suppressed in large volumes. We observe that these discretization effects are sufficiently small when the calculation is done with $m_q L \gtrsim 1$.

-
- [1] G. Martinelli, C. Pittori, C. T. Sachrajda, M. Testa, and A. Vladikas, “A General method for nonperturbative renormalization of lattice operators,” *Nucl. Phys.* **B445** (1995) 81–108, [arXiv:hep-lat/9411010](#) [[hep-lat](#)].
 - [2] G. Martinelli, G. C. Rossi, C. T. Sachrajda, S. R. Sharpe, M. Talevi, and M. Testa, “Nonperturbative improvement of composite operators with Wilson fermions,” *Phys. Lett.* **B411** (1997) 141–151, [arXiv:hep-lat/9705018](#) [[hep-lat](#)].
 - [3] V. Gimenez, L. Giusti, S. Guerriero, V. Lubicz, G. Martinelli, S. Petrarca, J. Reyes, B. Taglienti, and E. Trevigne, “Non-perturbative renormalization of lattice operators in coordinate space,” *Phys. Lett.* **B598** (2004) 227–236, [arXiv:hep-lat/0406019](#) [[hep-lat](#)].
 - [4] K. Cichy, K. Jansen, and P. Korcyl, “Non-perturbative renormalization in coordinate space for $N_f = 2$ maximally twisted mass fermions with tree-level Symanzik improved gauge action,” *Nucl. Phys.* **B865** (2012) 268–290, [arXiv:1207.0628](#) [[hep-lat](#)].
 - [5] K. G. Chetyrkin and A. Maier, “Massless correlators of vector, scalar and tensor currents in position space at orders α_s^3 and α_s^4 : Explicit analytical results,” *Nucl. Phys.* **B844** (2011) 266–288, [arXiv:1010.1145](#) [[hep-ph](#)].
 - [6] S. J. Brodsky, G. P. Lepage, and P. B. Mackenzie, “On the Elimination of Scale Ambiguities in Perturbative Quantum Chromodynamics,” *Phys. Rev.* **D28** (1983) 228.
 - [7] M. A. Shifman, A. I. Vainshtein, and V. I. Zakharov, “QCD and Resonance Physics. Theoretical Foundations,” *Nucl. Phys.* **B147** (1979) 385–447.
 - [8] R. C. Brower, H. Neff, and K. Orginos, “Mobius fermions: Improved domain wall chiral fermions,” *Nucl. Phys. Proc. Suppl.* **140** (2005) 686–688, [arXiv:hep-lat/0409118](#) [[hep-lat](#)]. [[686\(2004\)](#)].

- [9] R. C. Brower, H. Neff, and K. Orginos, “The Mobius Domain Wall Fermion Algorithm,” [arXiv:1206.5214 \[hep-lat\]](#).
- [10] D. B. Kaplan, “A Method for simulating chiral fermions on the lattice,” *Phys. Lett.* **B288** (1992) 342–347, [arXiv:hep-lat/9206013 \[hep-lat\]](#).
- [11] Y. Shamir, “Chiral fermions from lattice boundaries,” *Nucl. Phys.* **B406** (1993) 90–106, [arXiv:hep-lat/9303005 \[hep-lat\]](#).
- [12] T. van Ritbergen, J. A. M. Vermaseren, and S. A. Larin, “The Four loop beta function in quantum chromodynamics,” *Phys. Lett.* **B400** (1997) 379–384, [hep-ph/9701390](#).
- [13] K. G. Chetyrkin, “Quark mass anomalous dimension to O (α_s^4),” *Phys. Lett.* **B404** (1997) 161–165, [arXiv:hep-ph/9703278 \[hep-ph\]](#).
- [14] J. A. M. Vermaseren, S. A. Larin, and T. van Ritbergen, “The four loop quark mass anomalous dimension and the invariant quark mass,” *Phys. Lett.* **B405** (1997) 327–333, [arXiv:hep-ph/9703284 \[hep-ph\]](#).
- [15] D. J. Broadhurst and S. C. Generalis, “DIMENSION EIGHT CONTRIBUTIONS TO LIGHT QUARK QCD SUM RULES,” *Phys. Lett.* **B165** (1985) 175–180.
- [16] M. Jamin and M. Munz, “Current correlators to all orders in the quark masses,” *Z. Phys.* **C60** (1993) 569–578, [arXiv:hep-ph/9208201 \[hep-ph\]](#).
- [17] S. Narison and V. I. Zakharov, “Hints on the power corrections from current correlators in x space,” *Phys. Lett.* **B522** (2001) 266–272, [arXiv:hep-ph/0110141 \[hep-ph\]](#).
- [18] C. Morningstar and M. J. Peardon, “Analytic smearing of SU(3) link variables in lattice QCD,” *Phys. Rev.* **D69** (2004) 054501, [arXiv:hep-lat/0311018 \[hep-lat\]](#).
- [19] M. Luscher and P. Weisz, “On-Shell Improved Lattice Gauge Theories,” *Commun. Math. Phys.* **97** (1985) 59. [Erratum: *Commun. Math. Phys.* 98,433(1985)].
- [20] G. Cossu, J. Noaki, S. Hashimoto, T. Kaneko, H. Fukaya, P. A. Boyle, and J. Doi, “JLQCD IroIro++ lattice code on BG/Q,” in *Proceedings, 31st International Symposium on Lattice Field Theory (Lattice 2013)*. 2013. [arXiv:1311.0084 \[hep-lat\]](#).
- [21] M. C. Chu, J. M. Grandy, S. Huang, and J. W. Negele, “Correlation functions of hadron currents in the QCD vacuum calculated in lattice QCD,” *Phys. Rev.* **D48** (1993) 3340–3353, [arXiv:hep-lat/9306002 \[hep-lat\]](#).
- [22] **Particle Data Group** Collaboration, K. A. Olive *et al.*, “Review of Particle Physics,” *Chin. Phys.* **C38** (2014) 090001.

- [23] B. V. Geshkenbein, B. L. Ioffe, and K. N. Zybalyuk, “The Check of QCD based on the tau - decay data analysis in the complex q^{*2} - plane,” *Phys. Rev.* **D64** (2001) 093009, [arXiv:hep-ph/0104048](#) [hep-ph].
- [24] G. 't Hooft, “Computation of the Quantum Effects Due to a Four-Dimensional Pseudoparticle,” *Phys. Rev.* **D14** (1976) 3432–3450. [Erratum: *Phys. Rev.*D18,2199(1978)].
- [25] V. A. Novikov, M. A. Shifman, A. I. Vainshtein, and V. I. Zakharov, “Are All Hadrons Alike?,” *Nucl. Phys.* **B191** (1981) 301.
- [26] B. Fahy, G. Cossu, S. Hashimoto, T. Kaneko, J. Noaki, and M. Tomii, “Decay constants and spectroscopy of mesons in lattice QCD using domain-wall fermions,” in *Proceedings, 33rd International Symposium on Lattice Field Theory (Lattice 2015)*. 2015. [arXiv:1512.08599](#) [hep-lat].
- [27] G. Cossu, H. Fukaya, S. Hashimoto, T. Kaneko, and J. Noaki, “Stochastic calculation of the QCD Dirac operator spectrum with Mobius domain-wall fermion,” in *Proceedings, 33rd International Symposium on Lattice Field Theory (Lattice 2015)*. 2016. [arXiv:1601.00744](#) [hep-lat].
- [28] R. Narayanan and H. Neuberger, “Infinitely many regulator fields for chiral fermions,” *Phys. Lett.* **B302** (1993) 62–69, [arXiv:hep-lat/9212019](#) [hep-lat].
- [29] S. Aoki and Y. Taniguchi, “One loop calculation in lattice QCD with domain wall quarks,” *Phys. Rev.* **D59** (1999) 054510, [arXiv:hep-lat/9711004](#) [hep-lat].
- [30] H.-H. Zhang, K.-X. Feng, S.-W. Qiu, A. Zhao, and X.-S. Li, “On analytic formulas of Feynman propagators in position space,” *Chin. Phys.* **C34** (2010) 1576–1582, [arXiv:0811.1261](#) [math-ph].